

PASSIVE FORCE- DEFLECTION BEHAVIOR FOR ABUTMENTS WITH MSE CONFINED APPROACH FILLS

Prepared For:

Utah Department of Transportation Research
Division

Submitted By:

Brigham Young University
Department of Civil & Environmental
Engineering

Authored By:

Kyle M. Rollins, Travis M. Gerber
Luke Heiner

August 2010

THIS PAGE INTENTIONALLY LEFT BLANK

DISCLAIMER

The author alone is responsible for the preparation and accuracy of the information, data, analysis, discussions, recommendations, and conclusions presented herein. The contents do not necessarily reflect the views, opinions, endorsements, or policies of the Utah Department of Transportation, the US Department of Transportation or other agencies that provided funding for the project. The Utah Department of Transportation makes no representation or warranty of any kind, and assume no liability therefore.

THIS PAGE INTENTIONALLY LEFT BLANK

1. Report No. UT-10.15		2. Government Accession No.		3. Recipient's Catalog No.	
4. Title and Subtitle PASSIVE FORCE-DEFLECTION BEHAVIOR FOR ABUTMENTS WITH MSE CONFINED APPROACH FILLS				5. Report Date August 2010	
				6. Performing Organization Code	
7. Author Kyle M. Rollins, Travis M. Gerber, and Luke Hales				8. Performing Organization Report No.	
9. Performing Organization Name and Address Civil & Environmental Engineering Dept. Brigham Young University 368 CB Provo, UT 84602				10. Work Unit No. 5H06428H	
				11. Contract or Grant No. 06 9148	
12. Sponsoring Agency Name and Address Utah Department of Transportation 4501 South 2700 West Salt Lake City, Utah 84114-8410				13. Type of Report & Period Covered FINAL	
				14. Sponsoring Agency Code UT05.703	
15. Supplementary Notes Prepared in cooperation with the Utah Department of Transportation and Federal Highway Administration.					
16. Abstract <p>Approach fills behind bridge abutments are commonly supported by wrap-around mechanically stabilized earth (MSE) walls; however the effect of this geometry on passive force development is unknown. This report describes the first large-scale tests to evaluate passive force-deflection curves for abutments with MSE wingwalls. A test was also performed with fill extending beyond the edge of the abutment wall for comparison. The abutment wall was simulated with a pile supported cap 5.5 ft high, 11 ft wide, and 15 ft long in the direction of loading. The backfill behind the pile cap consisted of clean sand compacted to 96% of the modified Proctor maximum density. As the pile cap was loaded laterally, pressure on the MSE wall led to pull-out of the steel reinforcing grids and the MSE wall panels moved outward about 2% of the wall height when the ultimate passive force developed. Despite pullout, the passive force per effective width was 28 kips/ft for the pile cap with MSE wingwalls compared to 22.5 kips/ft for the cap without wingwalls. Nevertheless, the passive force with the MSE wingwalls was still only 76% of the resistance provided by the cap with fill extending beyond the edges. The pile cap with MSE walls required greater movement to reach the ultimate passive force (deflection of 4.2% of wall height vs. 3%). The Caltrans method provided good agreement with the measured passive resistance while the log spiral method required the use of a higher plane strain friction angle to provide reasonable agreement.</p>					
17. Key Words Passive Pressure, Bridge Abutment, MSE Walls, Earth Pressure, Load Test, Passive Force-Displacement Curves			18. Distribution Statement UDOT Research Division 4501 south 2700 West-box 148410 Salt Lake City, Utah 84114		23. Registrant's Seal
19. Security Classification (of this report) Unclassified		20. Security Classification (of this page) Unclassified		21. No. of Pages 83	22. Price

THIS PAGE INTENTIONALLY LEFT BLANK

ACKNOWLEDGEMENTS

This research investigation was supported by the Departments of Transportation for the states of California, Montana, New York, Oregon, and Utah through an FHWA pooled-fund arrangement, and the National Science Foundation under Award Number CMS-0421312, the George E. Brown, Jr. Network for Earthquake Engineering Simulation (NEES) which operates under NSF Award Number CMS-0402490. The support is greatly appreciated. The Utah Dept. of Trans. served as the lead agency with Daniel Hsiao as the Project Manager.

THIS PAGE INTENTIONALLY LEFT BLANK

TABLE OF CONTENTS

DISCLAIMER.....i

ACKNOWLEDGEMENTS v

LIST OF TABLESix

LIST OF FIGURESxi

1.0 INTRODUCTION..... 1

 1.1 Background..... 1

 1.2 Research Objectives..... 2

 1.3 Project Scope 2

2.0 TEST LAYOUT, INSTRUMENTATION, AND TESTING PROCEDURE5

 2.1 Test on Backfill Confined with MSE Wing Walls 5

 2.1.1 Test layout and Wall Geometry 5

 2.1.2 Instrumentation 8

 2.1.3 Load Test Procedure 14

 2.2 Test on Backfill without MSE Walls 15

3.0 GEOTECHNICAL SITE CHARACTERIZATION AND BACKFILL PROPERTIES 17

 3.1 Site Location 17

 3.2 Geotechnical Site Conditions..... 18

 3.3 Backfill Characteristics..... 22

4.0 STATIC TEST RESULTS AND DISCUSSION.....27

 4.1 Backfill Behavior 27

 4.2 Measured Total and Passive Force-Deflection Curves..... 29

4.3	Pressure Distribution on Pile Cap Face	31
4.3.1	Pressure Distribution for Backfill with MSE Wing Walls.....	31
4.3.2	Pressure Distribution for Backfill without MSE Wing Walls (Unconfined).....	33
4.4	Results from Strain Gauges on MSE Steel Grid Reinforcements	36
4.5	Compressive Movement of the Backfill and Transverse Movement of the MSE Wall.....	39
5.0	COMPARISON WITH COMPUTED FORCE-DISPLACEMENT RESPONSE	47
6.0	RESPONSE TO CYCLIC AND DYNAMIC LOADINGS.....	53
7.0	CONCLUSIONS.....	59
8.0	RECOMMENDATIONS	61
9.0	REFERENCES.....	63
	Appendix	65
A.	Calculation showing factor of safety for MSE wall grid against pull-out failure.....	65

LIST OF TABLES

Table 3-1 Backfill soil properties	24
Table 5-1 Comparison of measured and computed peak horizontal passive force.....	48

THIS PAGE INTENTIONALLY LEFT BLANK

LIST OF FIGURES

Figure 2-1 (a) Plan view and (b) elevation view of MSE wall confined soil backfill test layout and instrumentation.....	6
Figure 2-2 Photograph of MSE wall test construction.....	7
Figure 2-3 Photograph of MSE wall test construction nearing completion.....	7
Figure 2-4 Photograph of the reaction foundation.....	9
Figure 2-5 Plans for wall panels and connection details (SSL, Inc. 2009).....	10
Figure 2-6 Plans for wall panels and connection details (SSL, Inc. 2009).....	11
Figure 2-7 Schematic drawing of pressure plate in cap face with ID tags	12
Figure 2-8 Photograph of pressure plates in pile cap face	13
Figure 2-10 Photograph of strain gauge attached to steel grid	14
Figure 2-9 Schematic showing general strain gauge placement on MSE wall steel grids	14
Figure 2-11 Elevation view of the unconfined backfill test layout.....	15
Figure 3-1 Aerial photograph of test site	17
Figure 3-2 Location of test borings and CPT soundings relative to test foundation	19
Figure 3-3 Generalized soil profile along with results from CPT sounding near pile cap	20
Figure 3-4 Generalized soil profile and plots of typical soil properties for test site.....	21
Figure 3-5 Grain size distribution curves for backfill soil.....	23
Figure 3-6 Dry density histogram for the MSE wall test.....	24
Figure 3-7 Dry density histogram for the unconfined backfill test.....	25
Figure 3-8 Location of previous subsurface testing (Christensen 2006)	25
Figure 4-1 Observed cracking and vertical patterns at maximum displacement	28
Figure 4-2 Total, baseline and passive force verses deflection curves for pile cap for (a) MSE wall test (b) unconfined backfill test.....	30
Figure 4-3 Pile cap test with MSE wing walls: (a) Pressure versus depth curves for various displacement increments and (b) comparison of force-displacement curves with force	

obtained from the actuators and with force computed from the pressure plates times the tributary area	32
Figure 4-4 Pile cap test without MSE wing walls: (a) Pressure versus depth curves for various displacement increments and (b) comparison of force-displacement curves with force obtained from the actuators and with force computed from the pressure plates times the tributary area using actual width (11 ft) and effective width (18 ft).....	34
Figure 4-5 Schematic plan view drawing of pile cap showing stress concentrations at edges of the cap due to shear zones extending beyond the end of the cap and increasing the effective cap width.....	35
Figure 4-6 Summary of steel reinforcing grid force versus distance from the wall panel connection in comparison to the theoretical design pull-out force for top and bottom grids at pile cap displacements of 0.61, 1.99, and 3.51 inches.	37
Figure 4-8 Photograph of string potentiometers attached to steel stakes in backfill	39
Figure 4-7 Schematic drawing showing how increased lateral pressure would be produced on the MSE wall as a result of longitudinal displacement and passive pressure development on the pile cap	39
Figure 4-9 Longitudinal displacement of soil backfill as a function of initial distance from the pile cap face as the pile cap displaced longitudinally for MSE wall test.....	40
Figure 4-10 Longitudinal displacement of soil backfill for the MSE confined backfill (dashed lines) and unconfined backfill (solid lines) as a function of initial distance from the pile cap face as the pile cap deflected longitudinally.	41
Figure 4-11 Displacement of the MSE wall panels transverse to the direction of loading as a function of distance from the pile cap face.....	42
Figure 4-12 Compressive soil strain in the backfill confined by an MSE wing wall at various pile cap displacement levels.....	43
Figure 4-13 Compressive soil strain in the unconfined backfill at various pile cap displacement levels	43
Figure 4-14 Comparison of compressive strain in the soil as a function of distance from the pile cap face for several pile cap displacement intervals (MSE confined backfill strain is shown with dashed lines while curves for unconfined backfill are shown with solid lines)	45
Figure 5-1 Comparison of measured and computed passive force versus deflection relationships for backfill without MSE walls (Calculations used triaxial friction angle).....	50

Figure 5-2 Comparison of measured and computed passive force versus deflection relationships for backfill confined by MSE wing walls (Calculations used plane strain friction angle)50

Figure 6-1 Summary of pile cap response to cyclic actuator loadings with either the MSE walled backfill or with the backfill extending beyond the edges of the pile cap55

Figure 6-2 Summary of pile cap response to dynamic shaker loadings with either an MSE walled backfill or with backfill extending beyond the pile cap edge57

THIS PAGE INTENTIONALLY LEFT BLANK

EXECUTIVE SUMMARY

Approach fills behind bridge abutments are commonly supported by wrap-around mechanically stabilized earth (MSE) walls; however the effect of this geometry on passive force development is unknown. This report describes the first large-scale tests to evaluate passive force-deflection curves for abutments with MSE wingwalls. A test was also performed with fill extending beyond the edge of the abutment wall for comparison. The abutment wall was simulated with a pile supported cap 5.5 ft high, 11 ft wide, and 15 ft long in the direction of loading. The backfill behind the pile cap consisted of clean sand compacted to 96% of the modified Proctor maximum density. As the pile cap was loaded laterally, pressure on the MSE wall led to pull-out of the steel reinforcing grids and the MSE wall panels moved outward about 2% of the wall height when the ultimate passive force developed. The wall pull-out led to a somewhat irregular much softer force-displacement curve than is presently used in design. In addition, current design approaches do not explicitly account for the increased pressure on the MSE for this situation. Concrete wing walls at the edge of the abutment would eliminate this problem but they are not used in all designs.

Despite pullout, the ultimate passive force per effective width was significantly higher for the pile cap with MSE wing walls (28 kips/ft) compared to that for the cap without wing walls (22.5 kips/ft). Nevertheless, the passive force with the MSE wing walls was still only 76% of the resistance provided by the cap with fill extending beyond the edges. The measured ultimate passive force was best estimated using the log-spiral method, as recommended by AASHTO code provisions, but it was necessary to use the plane strain friction angle when computing the passive force for the MSE walls. For practical purposes, the plane strain friction angle can be estimated by increasing the triaxial friction angle by 10%. This typically increases the friction angle by 3 to 4 degrees and substantially increases the passive force on the abutment. The Caltrans method for predicting passive force also provided a reasonable prediction of the passive force on the pile cap with MSE wing walls.

Pull-out of the MSE reinforcement produced an irregular passive force-displacement curve that was significantly softer than expected based on curve design approaches. The pile cap with MSE walls required greater movement to reach the ultimate passive force (deflection of

4.2% of wall height vs. 3%) relative to the pile cap without wing walls. Additional tests are necessary to develop a design method to account for the additional force on the MSE wing wall reinforcements produced by loads on the abutment.

The actuator load tests indicate that damping ratios between 15 and 20% could be expected for dynamic loading of the abutment. These results are somewhat higher than the 10% value allowed in some design codes.

1.0 INTRODUCTION

1.1 Background

Passive force-deflection curves play a significant role in seismic design of bridge abutments. Numerical analyses conducted by El-Gamal and Siddharthan (1998), Faraji et al. (2001), and Shamshabadi et al. (2007) indicate significant influences of abutment stiffness on bridge response. Several large-scale tests have been conducted to gather data to quantify this relationship so that the results may be used in improved design models (Rollins and Cole 2006, Rollins and Sparks 2002, Mokwa and Duncan 2001, Romstad et al. 1996). These tests have typically used a backfill which extends beyond the edges of the pile cap or abutment. Commonly, however, space constraints necessitate that wrap-around mechanically stabilized earth (MSE) walls be used which truncate the approach fill soil to the width of the bridge or abutment wall. This truncation reduces the effective width of the approach fill, which in turn tends to decrease the passive resistance on the abutment. In contrast, the reinforcing grids would tend to provide increased confinement to the soil backfill and increase the resistance.

Current design methods in the Federal Highway Administration's design manual (FHWA, 1999) do not address the effects on MSE wall design as a pile cap or abutment wall is loaded laterally and parallel to the length of the wall as would tend to occur during a seismic event. Current seismic design guidelines for MSE walls only consider inertial loading of the wall normal to its face. The design guideline uses an acceleration coefficient determined as function of the maximum ground acceleration that is multiplied by a given coefficient and the passive pressure on the wall. This study evaluates kinematic loading effects in which the load on the MSE wing wall is produced by longitudinal movement of the pile cap. In addition, the effect of the wing wall resistance on the longitudinal resistance of the pile cap is evaluated. A review of the literature indicates that these issues have not been previously studied. Therefore, this report describes the first large-scale test to assess the effects of MSE wing walls or side walls on the passive resistance provided by soils in approach fills. As a comparison, a test with backfill

extending beyond the edges of the pile cap abutment wall, subsequently referred to as an unconfined backfill, was also performed. Passive force-deflection curves were developed under static loading using two hydraulic actuators with capacities of 600 kips in compression and 450 kips in tension. The passive force-deflection curves were obtained by subtracting the response of the pile cap without backfill from the total force-deflection curves with backfill in place. The backfill for both tests consisted of relatively clean sand compacted to 96% of the modified Proctor maximum density. The heave and cracking patterns in the backfill during the progression of each test were documented as was the transverse outward movement of the MSE wall. In addition, the tensile force developed in the steel grid reinforcements was measured. This report focuses on the MSE tests and uses results from the test on the unconfined backfill to provide comparison.

The ultimate passive force obtained from the testing was compared with various methods for computing ultimate passive force, namely the Rankine, Coulomb, log spiral, and Caltrans methods. In addition, the measured passive force-deflection curves were compared with curves computed using hyperbolic methods (Duncan and Mokwa 2001; Shamsabadi et al 2007) and the Caltrans design method (Caltrans 2001).

1.2 Research Objectives

The research objectives of this study are as follows:

1. Define static passive-force deflection curves for abutments with MSE wing walls.
2. Evaluate the difference in resistance relative to conditions with no MSE wing walls and compare it to design methods used to predict ultimate resistance and force-deflection relationships.
3. Define dynamic stiffness and damping for abutments with MSE wing walls.

1.3 Project Scope

This report describes the first large-scale test and an analysis of its results to assess the effects of MSE wing walls on the passive resistance provided by soils in approach fills. The test consisted of laterally loading a full-scale concrete pile cap using two hydraulic actuators with

capacities of 600 kips in compression and 450 kips in tension. Concrete MSE wing walls were constructed behind the pile cap and parallel to the direction of loading such that when the pile cap was loaded it would push between the MSE walls into a compacted clean sand backfill. Data acquisition instrumentation was used to gather real time results of the behavior of the test setup which include load, deflection and strain.

As a comparison, a test with backfill extending beyond the edges of the pile cap abutment wall, subsequently referred to as an unconfined backfill, was also performed. The loading and instrumentation were similar to that of the test with the MSE wing walls.

Analyses of the results of the two tests were developed for comparison and generally include; heave and crack mapping of the backfill soil, total and passive force-deflection curves, pressure distribution on the face of the pile cap with depth, axial load developed in the MSE wall steel grid reinforcement, compressive displacement of the backfill soil, and transverse movement of the MSE walls. Also, the ultimate passive force obtained from the testing was compared with various methods for computing ultimate passive force, namely the Rankine, Coulomb, log spiral, and Caltrans methods. The measured passive force-deflection curves were compared with curves computed using hyperbolic methods (Duncan and Mokwa 2001; Shamsabadi et al 2007) and the Caltrans design method (Caltrans 2001).

In addition to static loading, fifteen cycles corresponding to a typical cap displacement of 1/8 inch were applied by the actuators at a frequency of 0.75 Hz. Immediately before or after cycling, an eccentric mass shaker applied a dynamic load of 100 kips at a frequency of 10 Hz at these specific increments. Since passive force-displacement relationships can be improved by considering the effects of damping of the system these dynamic loads were applied to quantify this effect.

THIS PAGE INTENTIONALLY LEFT BLANK

2.0 TEST LAYOUT, INSTRUMENTATION, AND TESTING PROCEDURE

2.1 Test on Backfill Confined with MSE Wing Walls

2.1.1 Test layout and Wall Geometry

Figure 2-1 shows a plan and elevation view of the test layout for the pile cap with backfill confined by MSE wing walls. Figure 2-2 and Figure 2-3 show photographs of the MSE wall test layout under construction. The abutment wall was simulated with a pile supported concrete cap 5.58 ft high, 11 ft wide and 15 ft long in the direction of loading which was backfilled to a height of 5.5 ft. The top of the pile cap was level with the surrounding ground elevation; therefore, an area behind the pile cap was excavated to permit the MSE walls to be constructed adjacent to the cap. The MSE wall panels were 12-ft x 5-ft x 6-in reinforced concrete. To match the height of the cap, pieces of 2x8 sawn lumber were used to extend the height of the wall panels by one-half foot. The MSE walls on each side of the cap and backfill consisted of two MSE wall panels oriented in the direction of loading. As constructed, the MSE walls on either side were 5.5 ft tall and 24 ft long. The bottoms of the panels were placed on timber 4x4s that laid flat on the web of a steel I-beam that was turned on its side. This structure acted as a leveling pad for the wall panels and maintained alignment on the soft bottom of the excavation. The top of the 4x4s were level with the bottom of the pile cap. The backfill material for the MSE wall was well graded sand which will be described in more detail in the next section. During the backfill construction

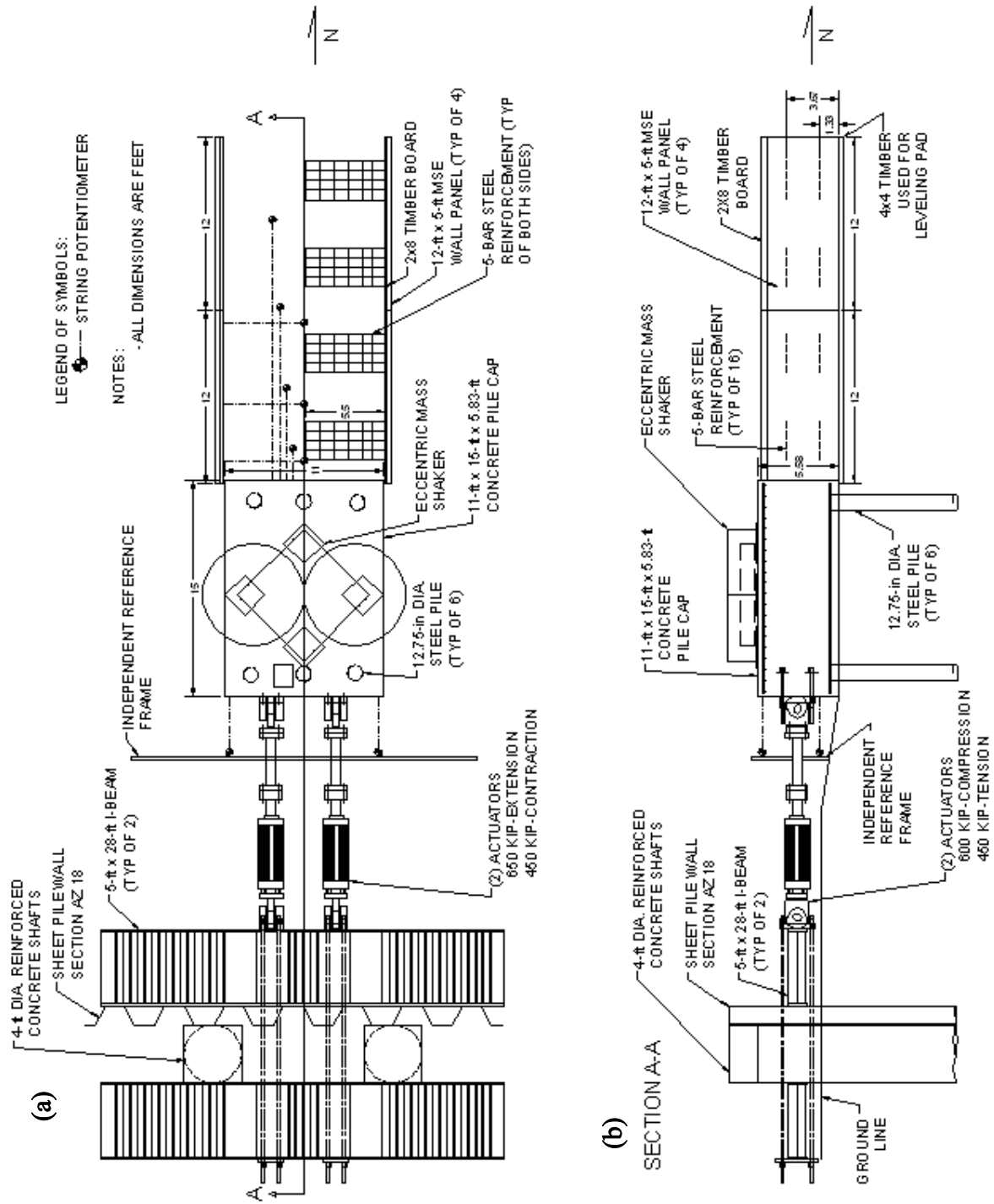


Figure 2-1 (a) Plan view and (b) elevation view of MSE wall confined soil backfill test layout and instrumentation



Figure 2-2 Photograph of MSE wall test construction



Figure 2-3 Photograph of MSE wall test construction nearing completion

process, two rows of galvanized steel reinforcing grid panels (4 grids per panel and 16 grids total) were placed at heights of 1.33 and 3.83 ft from the bottom of the wall. Typical panel and connection details are provided in Figure 2-5 and Figure 2-6 prepared by the wall supplier (SSL, Inc.). The steel grids consisted of five longitudinal bars (W11-3/8 inch diameter) spaced at 8 inches on centers to form a 32 inch wide panel, 5.5 ft long, or half the pile cap width. Transverse reinforcement bars (W8-5/16 inch) were welded to the longitudinal bars at 12 inch spacings on centers. The edge of the first grid was approximately 12 inches from the pile cap face. According to FHWA design methods, the overall panel factor of safety against pull-out was 1.45. However, the factor of safety against pull-out was 1.08 and 1.66 for the top and bottom steel grid reinforcement, respectively. See Appendix for factor of safety calculations.

2.1.2 Instrumentation

The pile cap was loaded by reacting off of a system of two 4-foot diameter reinforced concrete drilled shafts south of the concrete cap. The shaft lengths were 55.18 and 70 ft. In addition to the concrete shafts, a steel sheet pile wall was driven on the north side of the shafts and two steel I-beams used to integrate the system together with eight 2 1/2 inch diameter post-tensioned threaded bars. The steel sheet pile wall was an AZ-18 section, ASTM A-572 Grade 50 and was driven to approximately 33 1/2 to 34-foot depth. The steel I-beams were 64 in by 16 in by 30 ft long with web stiffeners to help distribute the load. A photograph of the reaction foundation can be seen in Figure 2-4.

Deflection data during testing was obtained using string potentiometers. Longitudinal movement of the pile cap was measured by four potentiometers at the four corners of one side of the pile cap from an independent reference frame. Measurements of the longitudinal backfill soil



Figure 2-4 Photograph of the reaction foundation

displacement at the ground surface were obtained from string potentiometers attached to the top of the pile cap and to metal stakes placed near the centerline of the sand backfill at distances of 2, 6, 12, and 16 ft behind the cap. This data was also used to compute backfill compressive strain versus distance from the cap. Vertical movement of the backfill was obtained by a level survey of the change in elevation of points on a 2-ft square grid that was painted on top of the backfill. Surveys were taken before loading and again at the maximum loading. The grid was also used to document crack patterns development during the test. Transverse movement of the MSE walls

was also measured. Three string potentiometers were located on the west MSE wall panel closest to the pile cap at distances of 1.33, 5.25, and 10.92 ft from the pile cap face. Load cells within each hydraulic actuator were used to measure the force applied to the pile cap and soil backfill system and then summed to obtain the total applied force.

Six 9 inch diameter pressure cells were used to measure the pressure distribution with depth from the backfill on the face of the pile cap. These pressure cells were placed with their centers at depths of 7.75, 18.5, 29.5, 41.0, 51.5, and 62.5 inches below the top of the pile cap in the center portion of the pile cap. Figure 2-7 and Figure 2-8 show a schematic drawing and photograph of the pressure cells in the face of the pile cap, respectively. These stainless steel pressure cells were designed with a reinforced backplate to reduce point loading effects when directly mounting the cell to a concrete or steel structure. The cells utilized a semi-conductor pressure transducer rather than a vibrating wire transducer to measure more accurately the rapidly changing pressures. The cells were cast integrally with the pile cap, with their top surfaces being flush with the concrete face.

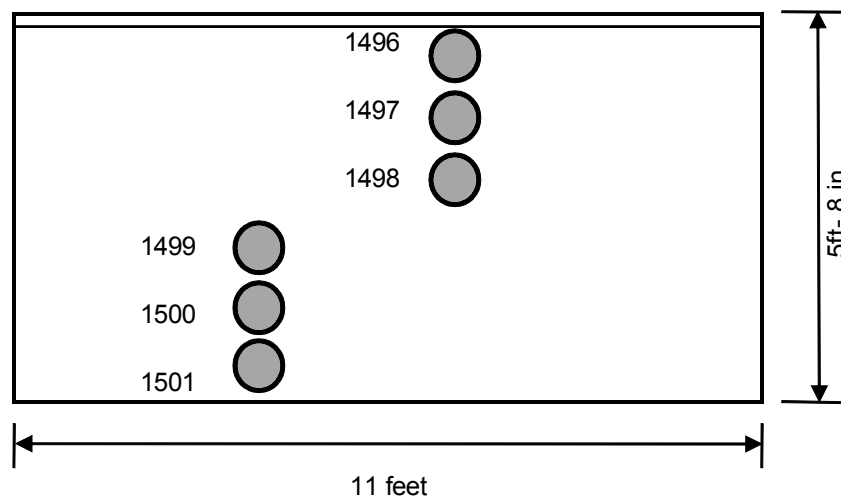


Figure 2-7 Schematic drawing of pressure plate in cap face with ID tags



Figure 2-8 Photograph of pressure plates in pile cap face

A total of 40 strain gauges were attached to the closest six steel grid panels on the east wall in an effort to measure the increase in axial force in the grid panels during lateral loading of the pile cap. Four of the instrumented grids were attached to the panel closest to pile cap, while the remaining two were attached to the top and bottom connections for the next panel. See Figure 2-9. The strain gauges were attached to the bottom side of the center longitudinal bar for each instrumented panel at varying locations from the grid to wall face connection. The placement locations were intended to capture the anticipated peak axial loads in the steel wire and to provide a detailed profile of axial load along its length. Therefore, the distances from the face of the wall to the strain gauges varied for the top and bottom grids. For the top steel grids, strain gauges were placed at distances of 2, 7, 12, 18, 30, 42 and 54 inches from the connection to the wall panel and in the bottom grids, strain gauges were located at 2, 4, 6, 9, 22, 35, and 48 inches from the wall panel connection. The remaining two grids on the next panel had six gauges per panel due to a shortage of data channels on the data acquisition equipment. The strain gauge spacing for the top steel grid was 2, 10, 18, 30, 42 and 54 inches from the wall face and the bottom steel grid spacing was 2, 6, 9, 22, 35 and 48 inches. The strain gauges were electrical

resistance type gauges rather than vibrating wire gauges to allow for rapid measurement of strain. Figure 2-10 shows an example of a strain gauge attached to the steel grid.

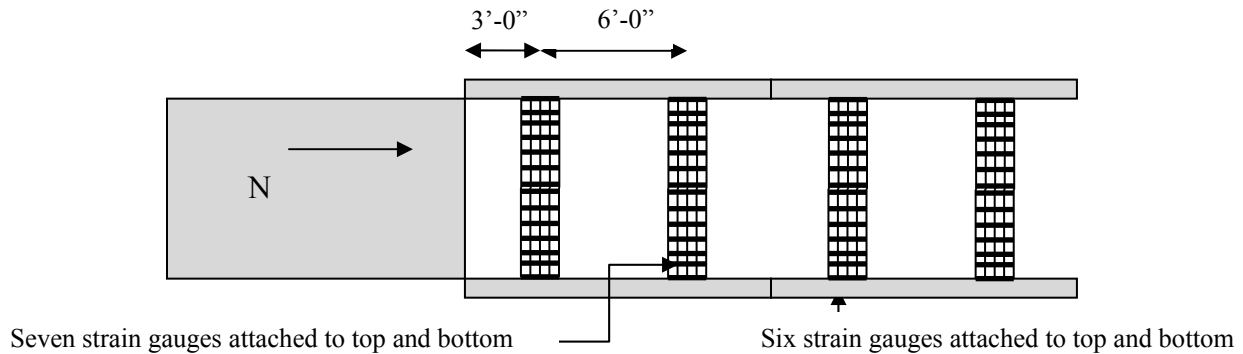


Figure 2-9 Schematic showing general strain gauge placement on MSE wall steel grids



Figure 2-10 Photograph of strain gauge attached to steel grid

2.1.3 Load Test Procedure

The procedure for the test was to load the pile cap with the hydraulic actuators in approximately 1/4 inch increments. The actual deflection increments used were: 0.20, 0.61, 0.68, 1.07, 1.30, 1.55, 1.75, 1.98, 2.27, 2.51, 2.76, 3.05, 3.30, and 3.51 inches. At increments 0.20, 0.61, 1.30, 1.98, 2.76, and 3.51, fifteen cycles corresponding to a typical cap displacement of 1/8 inch were applied by the actuators at a frequency of 0.75 Hz. An eccentric mass shaker was also used to apply a ramped dynamic load up to 100 kips at a frequency of 10 Hz. The first use of the actuators and shaker to apply cyclic and dynamic loads, respectively, was alternated between each test increment.

2.2 Test on Backfill without MSE Walls

Figure 2-11 provides an elevation view of the test setup for the unconfined backfill extending beyond the edges of the pile cap. The layout for the unconfined soil backfill test consisted of the same pile cap and reacting system. An area behind the pile cap was excavated below the bottom of the cap approximately one and a half feet for a distance of eight feet and then sloped at 1V:3.5H at an elevation equal to the bottom of the pile cap. This geometry was considered large enough to enclose the passive failure surface. The excavation extended five feet beyond the width of the pile cap to allow for 3D end effects of the failure wedge.

The testing procedure for this backfill condition followed a similar pattern as the MSE wall confined soil backfill test. The actual deflection increments were: 0.12, 0.26, 0.46, 0.64, 0.88, 1.19, 1.50, 1.80, 2.07, 2.27, and 2.50 inches. Cyclic and dynamic loadings were applied at displacement increments of 0.11, 0.26, 0.43, 0.63, 0.87, 1.18, 1.46, 1.81, 2.09, 2.24 and 2.52 during this test in the same manner as described above for the MSE wall test.

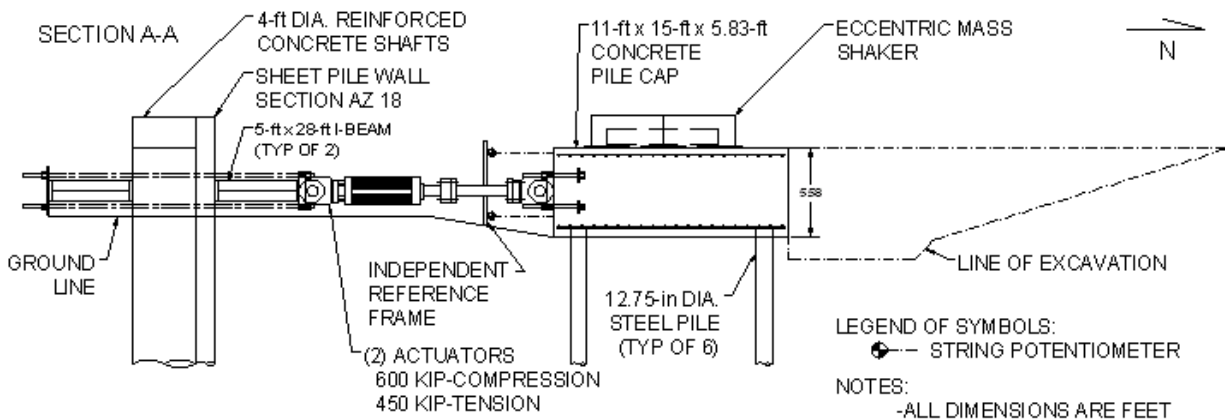


Figure 2-11 Elevation view of the unconfined backfill test layout

THIS PAGE INTENTIONALLY LEFT BLANK

3.0 GEOTECHNICAL SITE CHARACTERIZATION AND BACKFILL PROPERTIES

3.1 Site Location

The test site is at the Salt Lake City International Airport about 1000 ft north of the air traffic control tower as shown in Figure 3-1. This site is ideal site because it is flat and open which allows easy access for heavy equipment and there are no overhead obstructions or subsurface utilities. In addition, because of its location, the site is relatively secure. Finally, a number of field tests have been performed at this site over the past 15 years and the geotechnical investigations provide a great deal of information about the soil conditions at this location.

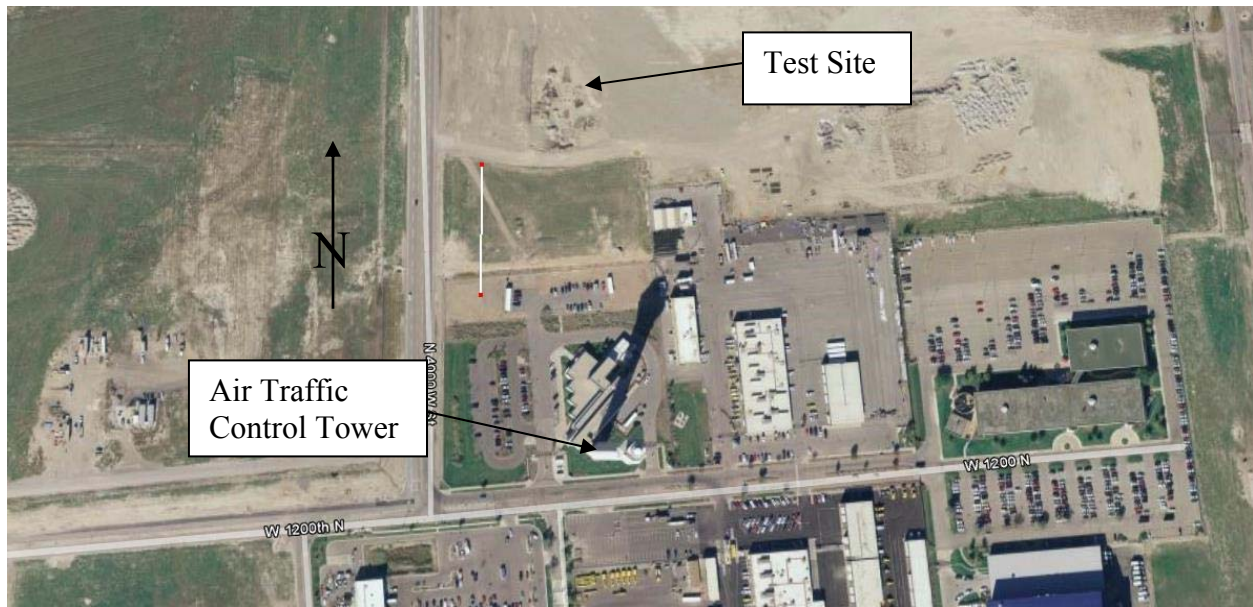


Figure 3-1 Aerial photograph of test site

3.2 Geotechnical Site Conditions

The soil profile in the vicinity of the test site originally consisted of a 5 ft thick layer of compacted sandy gravel fill overlying alternating layers of silty clay and sand to a depth of 100 ft. This gravel layer and approximately 3 ft of the underlying silty clay layer were excavated in 2004 and replaced with compacted sand, making the top layer of sand about 8 ft deep in the vicinity of the pile cap. A significant number of bore holes and cone penetration soundings have been made at the test site and their locations relative to the test foundations are shown in Figure 3-2. In addition to tests on undisturbed samples from the boreholes, a number of in-situ tests have been performed including standard penetration tests, vane shear tests, pressuremeter tests, shear wave velocity tests, and dilatometer tests. These test results are presented elsewhere, see Rollins and Peterson (1996), Snyder (2004), and Christensen (2006).

The profile at the location of the pile cap is best defined by sounding CPT-06-M which extended to a depth of about 70 ft. The cone tip resistance, sleeve friction, pore pressure and friction ratio obtained from this sounding are presented in Figure 3-3 along with an interpreted soil profile based on the CPT sounding and lab tests. Profiles showing results from additional testing including shear strength testing, shear wave velocity testing, and consolidation testing are provided relative to the soil profile in Figure 3-4.

Since laterally loaded piles typically receive most of their support from the soil in the upper 5 to 15 pile diameters, the shallow surface layers are of greatest interest for this study. The native cohesive surface soils consist of low-plasticity silts and clays classifying as ML, CL-ML or CL according to the Unified Soil Classification System (USCS). Hydrometer analyses

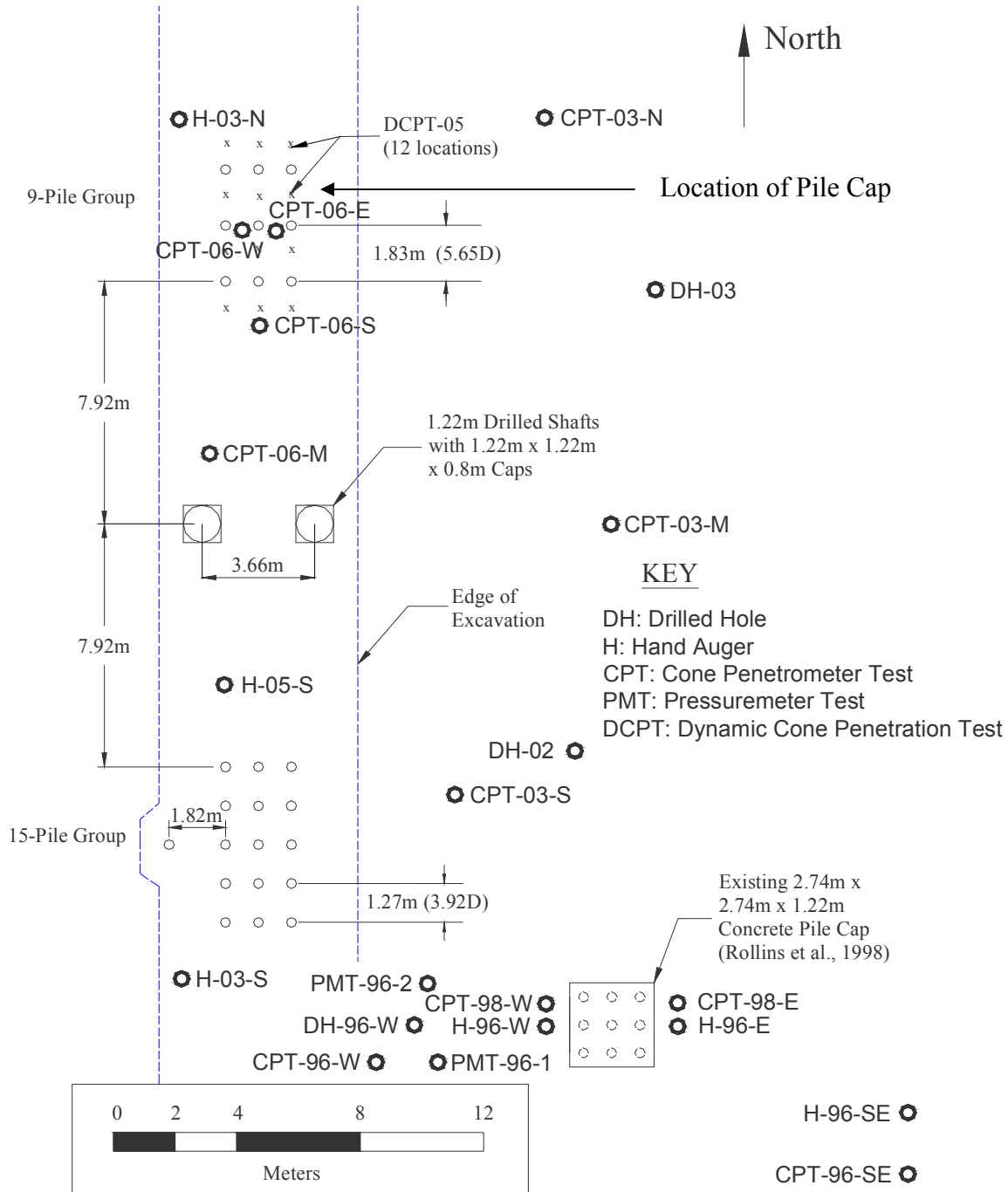


Figure 3-2 Location of test borings and CPT soundings relative to test foundation

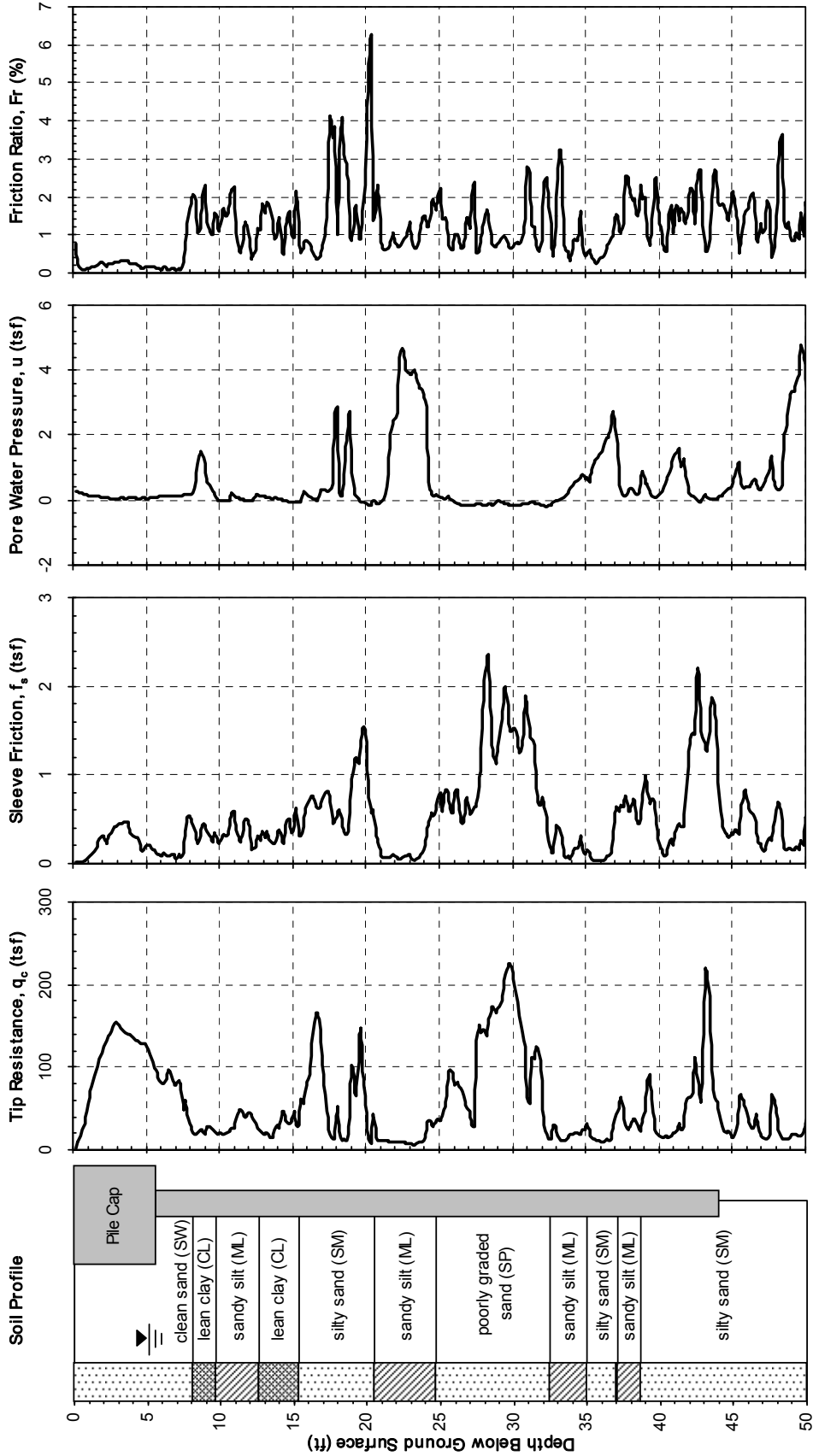


Figure 3-3 Generalized soil profile along with results from CPT sounding near pile cap

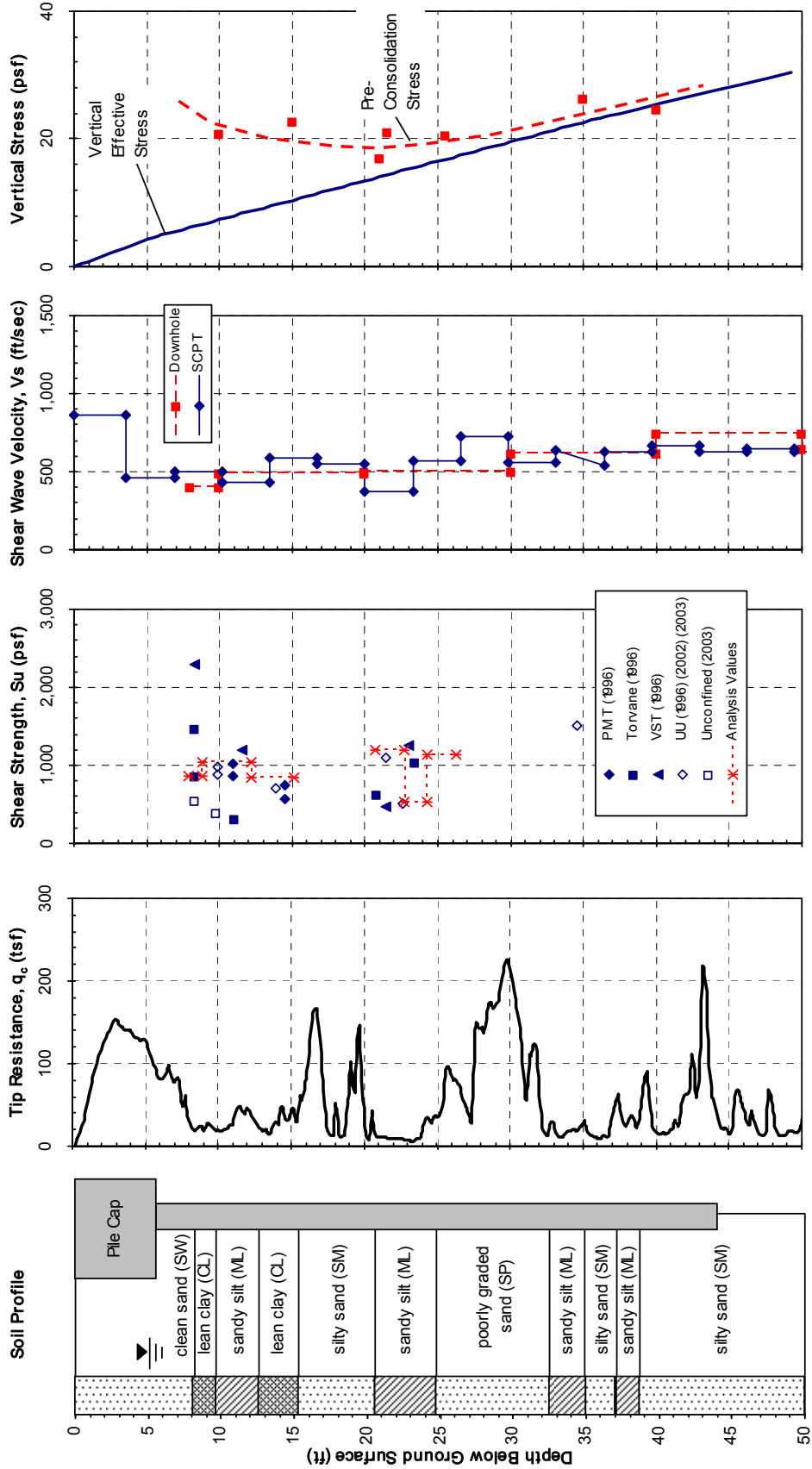


Figure 3-4 Generalized soil profile and plots of typical soil properties for test site

indicate that a majority (50 to 75%) of the cohesive soil near the ground surface consists of silt-size particles with a clay-size content generally between 10 and 25%. The undrained shear strength is typically between 500 and 1000 psf, although some layers had strengths of 2000 psf as shown in Figure 3-4. A design strength profile is also shown in Figure 3-4. The strength would be expected to increase with depth in a relatively linear manner. However, near the ground surface the soils exhibit much higher strengths due to overconsolidation by desiccation. The consolidation testing indicates that the soils are overconsolidated to a depth of about 30 ft. The underlying cohesionless soil layer consists of poorly graded medium-grained sands and silty sands classifying as SP or SM according to the USCS. SPT blow counts and CPT tip resistances indicate that the sand is dense to very dense with corresponding relative densities (D_r) of 65 to 85%. The measured shear wave velocity was 860 ft/sec in the compacted fill from 0 to 4 ft below the natural ground surface and then decreased to between 400 and 600 ft/sec in the native soils from 5 ft to 15 ft in depth. Agreement between the downhole and seismic cone penetration test results is relatively good. The water table was located at a depth of about 5.5 ft during the testing.

3.3 Backfill Characteristics

The backfill material used for both the MSE wall test and the unconfined backfill test was a clean well graded sand classifying as SW material according to the Unified Soil Classification System (USCS). Two gradation curves are provided in Figure 3-5 along with an average curve. Typical gradation properties are summarized in Table 3-1. The sand contains less than 5% fines and generally fits within a concrete sand (ASTM C33) gradation range. The maximum Proctor dry unit weight was 111 lb/ft³ with an optimum moisture content of 11%. However, because of the low fines content the water content had relatively little effect on the compaction efficiency

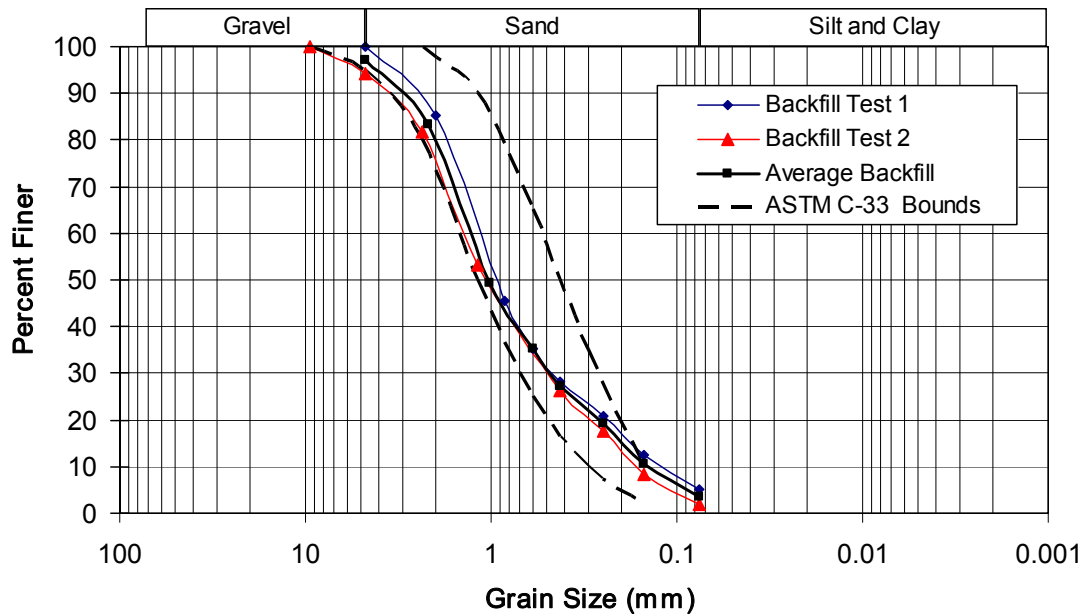


Table 3-1 Backfill soil properties

D_{60}	1.3 mm
D_{50}	1.0 mm
D_{30}	0.7 mm
D_{10}	0.3 mm
C_u	8.57
C_c	1.49
e_{max}	0.96
e_{min}	0.48
γ_{max}	113.3 pcf
γ_{min}	85.3 pcf
Modified Proctor γ_{max}	111 pcf @11%

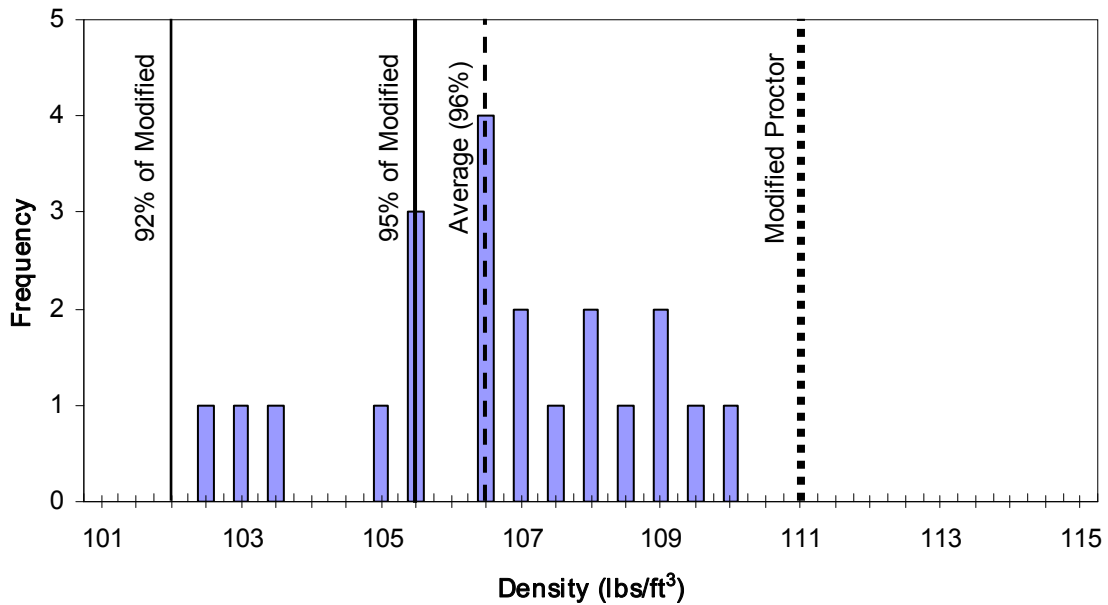


Figure 3-6 Dry density histogram for the MSE wall test

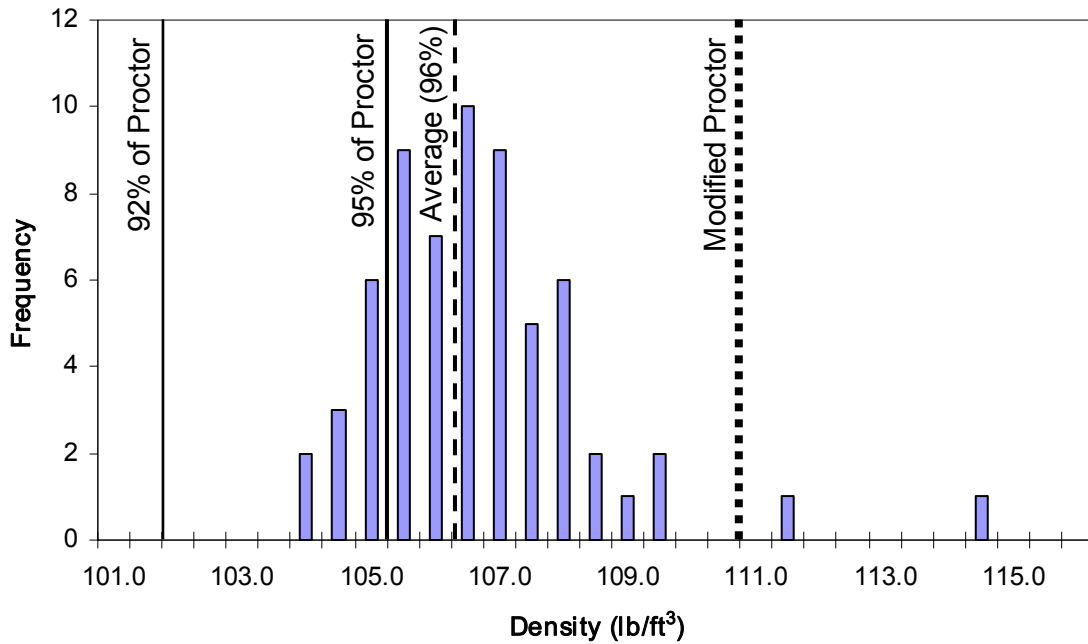


Figure 3-7 Dry density histogram for the unconfined backfill test

minimum and maximum void ratios in Table 3-1, the mean relative density of the sand backfill was about 80%.

A direct shear test was performed on 3 test specimens with the gradation shown by gradation 1 in Figure 3-5. These samples were compacted to 96% of the modified Proctor maximum density at a moisture content of 8%. The soil was then sheared at this moisture content to simulate field conditions. This test yielded a friction angle of 39° with zero cohesion. Further, a direct shear test was performed on four specimens with gradations corresponding to gradation 2 in Figure 3-5. This series of tests indicated a peak friction angle of 43.3° with an ultimate friction angle of 40.5°. For this study we have assumed a friction angle of 40.5° for the combined average gradation with essentially zero cohesion.

THIS PAGE INTENTIONALLY LEFT BLANK

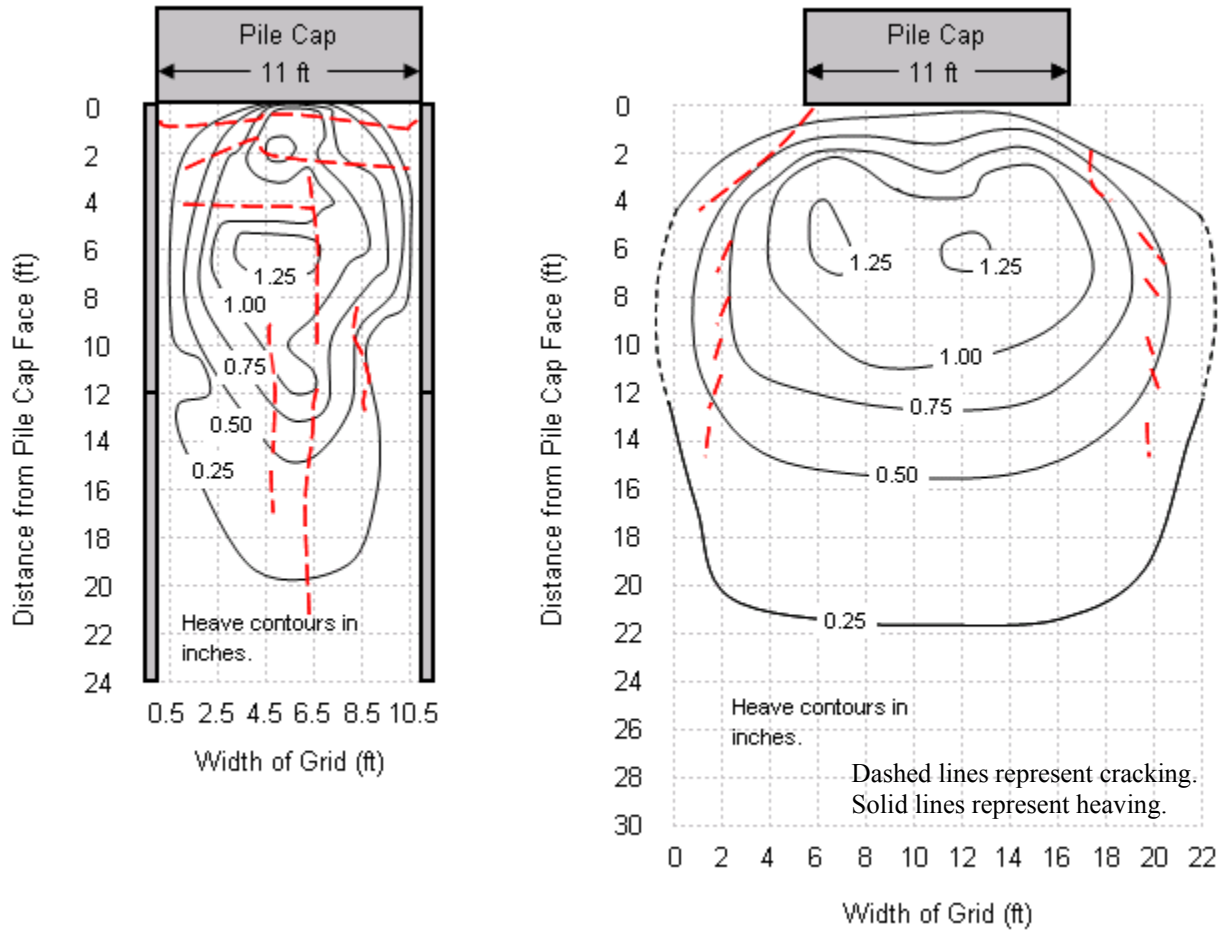
4.0 STATIC TEST RESULTS AND DISCUSSION

Test results presented in this report are organized in the following manner. First, plots of the observed backfill cracking and vertical heaving patterns for each test are provided. Next plots of the static total and passive force-displacement curves for the backfill confined by MSE wing walls as well as for the unconfined backfill without walls are provided. Then the pressure distribution on the pile cap face is presented along with the passive force interpreted from these measurements for both tests. Next, plots of the tensile force in the steel reinforcing grids are presented. Next, the longitudinal backfill displacement and interpreted compressive strain data for each backfill are presented and compared as a function of distance behind the pile cap for a number of longitudinal pile cap displacements. Finally, the transverse or outward movements of the MSE wall panels are presented as a function of distance behind the pile cap for a number of longitudinal pile cap displacements.

4.1 Backfill Behavior

Surface cracking of the soil backfill was observed during the progression of each test. Figure 4-1 shows the observed cracking, shown as dashed lines, and vertical heave contours, shown as solid lines, at the maximum displacement associated with both tests. As noted previously, a 2-ft square grid was painted on the backfill to help identify and document the cracking. The amount of vertical heave was measured with surveying equipment at the beginning and end of each test. The clean sand grain-characteristics and the cyclic and dynamic loading made it difficult to observe smaller cracks in the surface of the backfill and contributed to some error in the heave measurements due to loosened sand on the surface being shifted by the dynamic loading. However, the larger, well defined cracks were noted and documented. For the MSE wall confined backfill, it was observed that cracking occurred both parallel and perpendicular to the

pile cap face. The parallel cracking occurred within 4 feet of the face of the cap while the perpendicular cracking occurred from 4 to 22 ft from the cap face. This observation is made



MSE Wall Test

Unconfined Backfill Test

Figure 4-1 Observed cracking and vertical patterns at maximum displacement

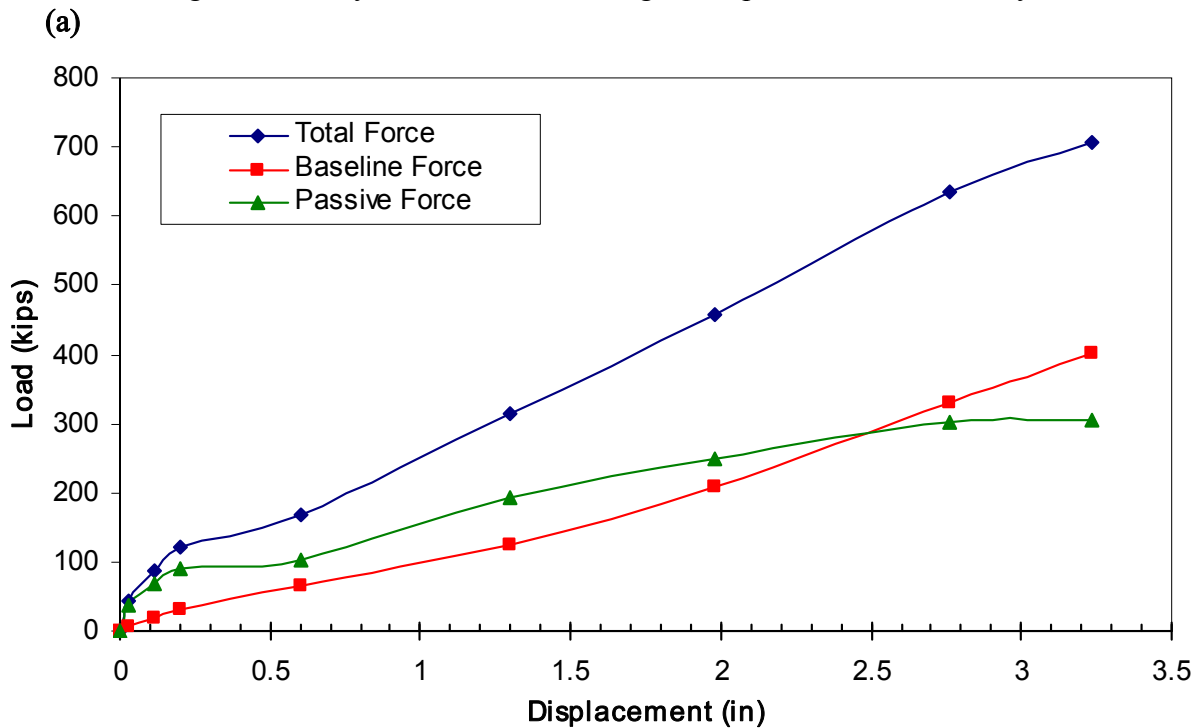
noting that the walls moved outward engaging the grid reinforcement allowing cracks to form parallel to the MSE panels.

For the unconfined backfill without MSE wing walls, radial cracking beginning near the corners of the pile cap developed out to a distance of little over 4 feet beyond the edges of the pile cap. This pattern is indicative of 3D end effects and resulted in an effective failure surface width of approximately 18 to 19 ft for the unconfined fill. Although there is a significant difference in the widths of the effective soil wedges, the maximum vertical heave for both tests

was approximately 1 1/4 inches and occurred 6 feet from the pile cap face near the center of the width of the backfill. Generally, the crack pattern for the pile cap without MSE walls is typical of a three-dimensional failure, while that for the backfill with MSE wing walls is more typical of a two-dimensional failure mechanism approaching a plane strain condition.

4.2 Measured Total and Passive Force-Deflection Curves

Figure 4-2 shows the total, baseline and passive force versus displacement curves for the backfill with and without MSE walls. Data points correspond to the deflection increments at which the cyclic and dynamic loadings also occurred as mentioned in the Test Layout and Procedure section. Since the static loads dropped after cycling and shaking, the corresponding loads represent a peak load at the given deflection. The curve connecting the data points is defined as the “backbone” curve. It may be observed that the force-displacement curves do not have the typical hyperbolic shape, but exhibit a swale in the middle. This intermediate plateau is likely due to several factors. First, the cyclic loading during each increment appears to have reduced the stiffness. In addition, for the small displacement increments involved it is possible that the reloading did not fully reach back to the virgin compression curve. Lastly, the transverse



(b)

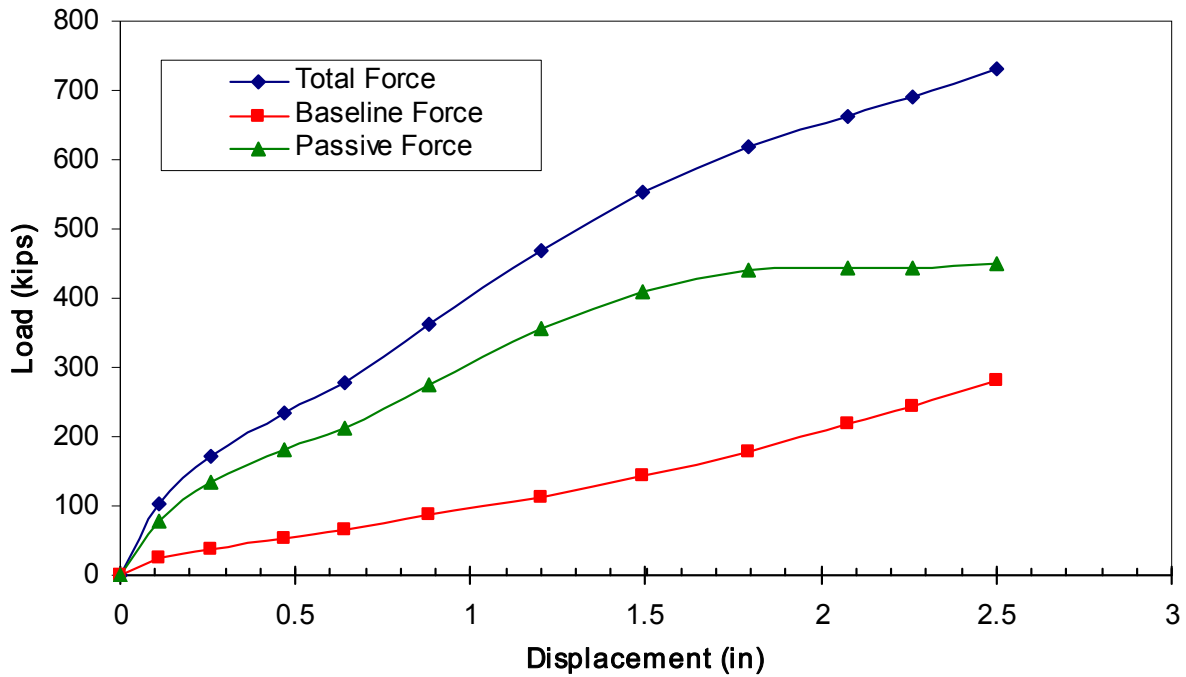


Figure 4-2 Total, baseline and passive force verses deflection curves for pile cap for (a) MSE wall test (b) unconfined backfill test

movement of the MSE walls loading appears to have led to a reduction in passive force as discussed in more detail subsequently. Figure 4-2 shows that at the maximum deflection of the unconfined backfill of 2.5 inches, the total resistance provided by the pile cap and backfill with MSE walls is 80% of the resistance provided by the pile cap with backfill extending beyond the edges at the same displacement, a 20% reduction in total resistance. As discussed subsequently, the decrease is a result of a smaller effective width as well as reduced soil stiffness. The passive resistance for each test was computed by subtracting the resistance provided by the pile cap system without backfill from the total resistance provided by the pile cap and backfill with and without MSE walls. It should be noted that this test setup was used to test a variety of different backfill materials and configurations including the dense sand backfill with and without MSE walls during the summer of 2007. The unconfined dense sand backfill test was conducted on May 25th while the MSE wall confined dense sand backfill test was performed on June 18th due to logistical constraints. The passive force-displacement curves for both tests were developed using the same baseline test without any backfill.

At the ultimate state, the backfill with MSE wing walls developed about 76% of the passive resistance provided by the backfill which extended beyond the edges of the pile cap. The increased passive force for the unconfined backfill appears to be largely attributable to the increased effective width of the pile cap. As noted previously, surface shear zones extended over 3 to 4 ft beyond the edge of each side of the cap, effectively increasing the pile cap width from 11 ft to approximately 18 to 19 ft. Assuming an effective width of 18 ft for the unconfined backfill, the ultimate passive force per effective width was 28 kips/ft for the MSE confined backfill and only 25 kips/ft for the unconfined backfill. The higher passive force per width can be attributed to confinement provided by the MSE wall and the fact that the failure surface was constrained to develop under more or less plane strain conditions. The ultimate passive resistance occurred at pile cap deflections equal to 4.2% and 3.0% of the wall height for the MSE-confined and unconfined backfill tests, respectively. This deflection level for the MSE wall test is somewhat greater than the 3.0 to 3.5% range for full-scale lateral pile cap tests in dense sands and gravels reported by Rollins and Cole (2006).

4.3 Pressure Distribution on Pile Cap Face

4.3.1 Pressure Distribution for Backfill with MSE Wing Walls

The measured pressure distribution with depth for the test with MSE wing walls is plotted in Figure 4-3 (a) for six pile cap displacement increments. As the displacement increases, the pressure increases; however, relatively little change is observed for displacements higher than about 1.98 inches when the maximum load is developed. The pressure distribution tends to have a bilinear shape with a lower slope at the top than at the bottom. This could result from lower confinement at the top of the wall due to pull-out of the MSE reinforcement or outward rotation of the MSE wall as discussed subsequently.

The force on the pile cap was computed by multiplying the pressure at each measurement elevation by the tributary area. The tributary area is the width of the pile cap times the vertical distance between pressure plates. The total force on the pile cap computed from the pressure plates is compared with the force measured by the actuators in the force-displacement curves plotted in Figure 4-3 (b). The two curves generally have similar shapes, although the force from

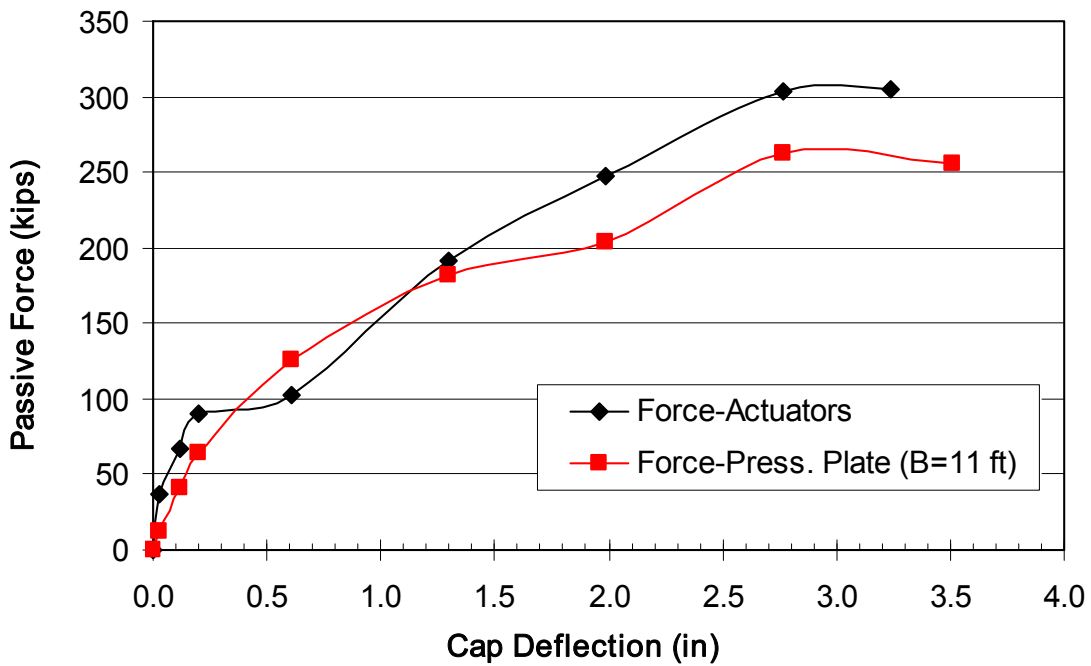
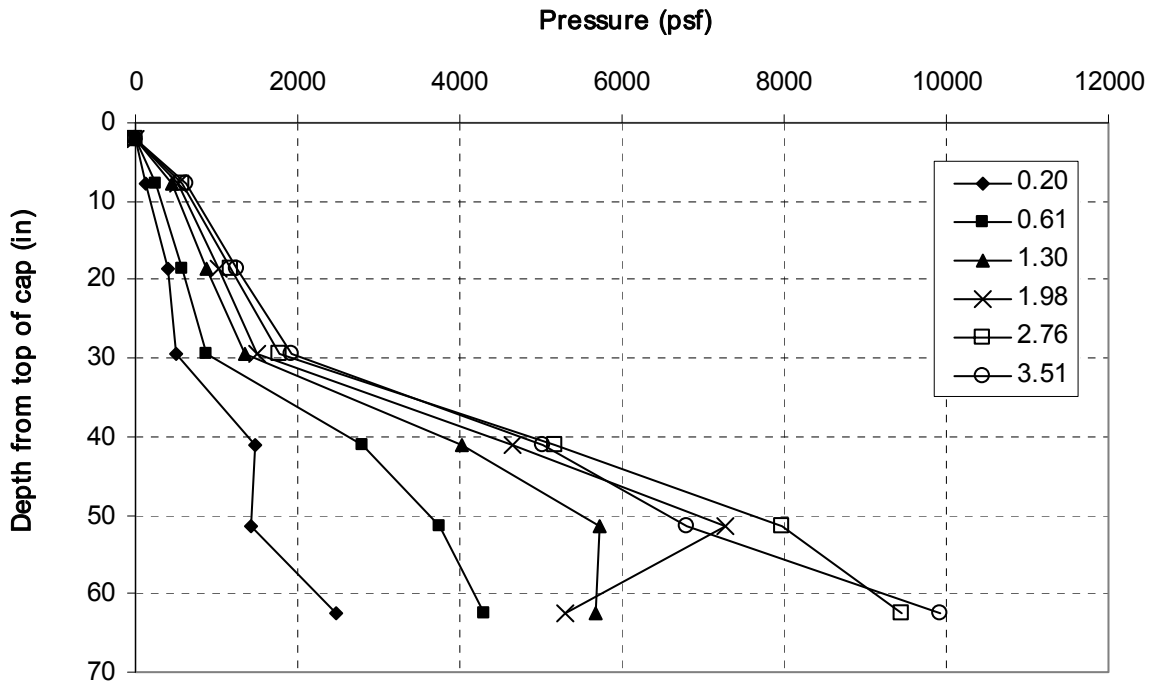


Figure 4-3 Pile cap test with MSE wing walls: (a) Pressure versus depth curves for various displacement increments and (b) comparison of force-displacement curves with force obtained from the actuators and with force computed from the pressure plates times the tributary area

the actuators is about 15 to 20% higher than that from the pressure plates. This discrepancy can likely be attributed to the assumption of uniform pressure across the width of the pile cap. Soil-structure analyses typically show stress concentrations near the ends of a concrete mat or pile cap. Since the pressure plates are near the center of the cap, they would not register this increased pressure near the ends and would, therefore, underestimate the total force on a horizontal segment of the pile cap.

4.3.2 Pressure Distribution for Backfill without MSE Wing Walls (Unconfined)

The measured pressure distribution with depth for the test without MSE wing walls is plotted in Figure 4-4 (a) for eleven pile cap displacement increments. As the displacement increases, the pressure increases; however, smaller increases are observed at higher displacements as the maximum load is approached. The pressure distribution tends to have a parabolic shape and there is a reduction in pressure at the base of the cap which suggests pile cap rotation.

The force on the pile cap was computed by multiplying the pressure at each measurement elevation by the tributary area as described previously. The total force on the pile cap computed from the pressure plates is compared with the force measured by the actuators in the force-displacement curves plotted in Figure 4-4 (b). The two curves generally have similar shapes; however, the force from the actuators is about 30% to 50% higher than that from the pressure plates. This is significantly more error than that observed for the pile cap with the MSE wing walls. Once again, this discrepancy can likely be attributed to the assumption of uniform pressure across the width of the pile cap. Because the shear zones extend beyond the ends of the pile cap without wing walls, greater stress concentrations would be expected to develop at the ends of the pile cap as illustrated in Figure 4-5. Since the pressure plates are near the center of

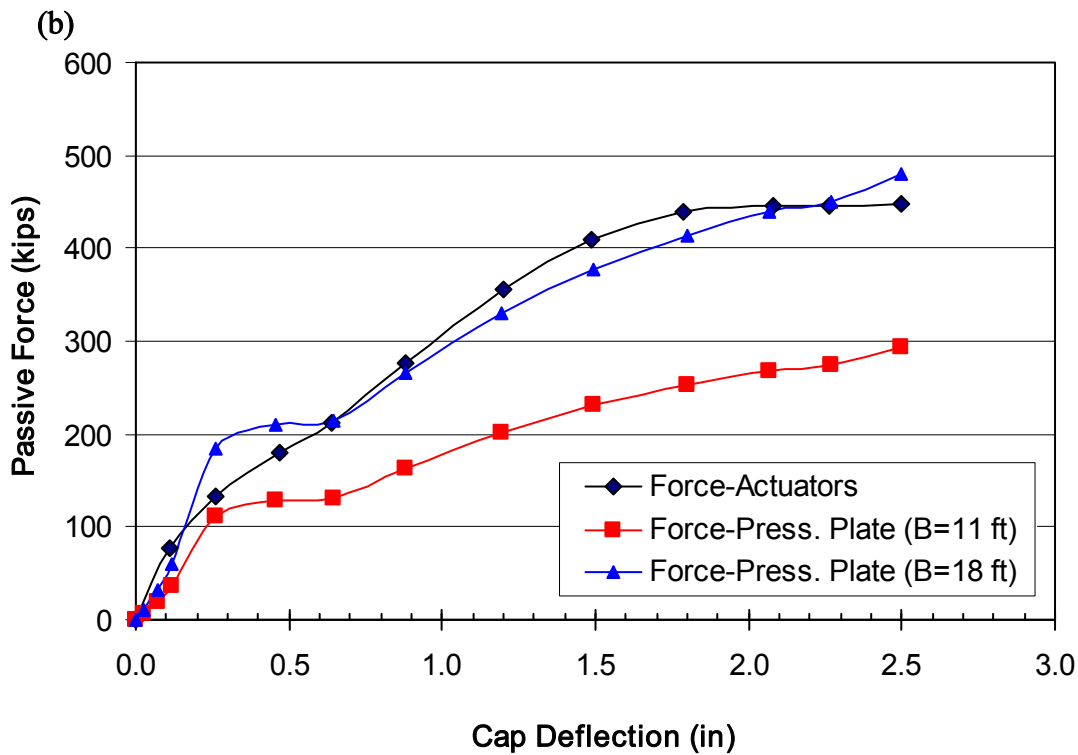
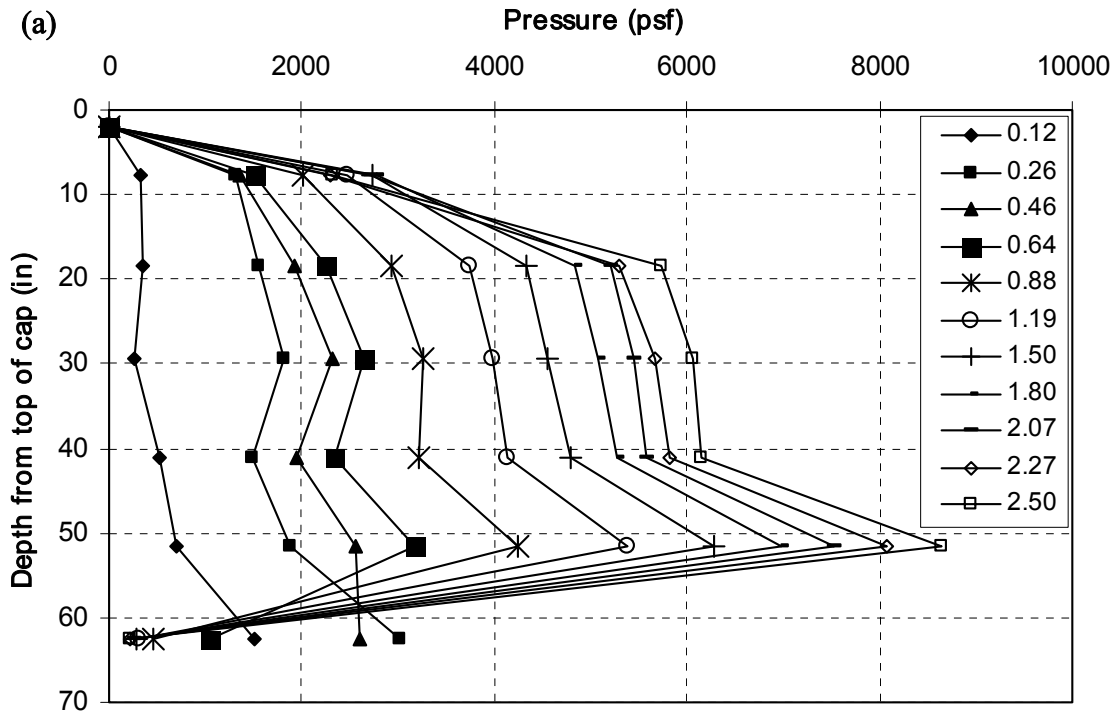


Figure 4-4 Pile cap test without MSE wing walls: (a) Pressure versus depth curves for various displacement increments and (b) comparison of force-displacement curves with force obtained from the actuators and with force computed from the pressure plates times the tributary area using actual width (11 ft) and effective width (18 ft)

the cap, they would not register this increased pressure near the ends and would, therefore, underestimate the total force on a horizontal segment of the pile cap. One method to account for the increased passive resistance due to 3-D end effects is to increase the effective width of the pile cap. The Brinch-Hansen equation and field observations suggest that the effective width of the pile cap for this geometry is approximately 18 ft, rather than the actual 11 ft cap width. When an effective cap width of 18 ft is used, the agreement between the total passive force computed from the pressure plates is reasonably close to that measured by the actuators as shown in Figure 4-4.

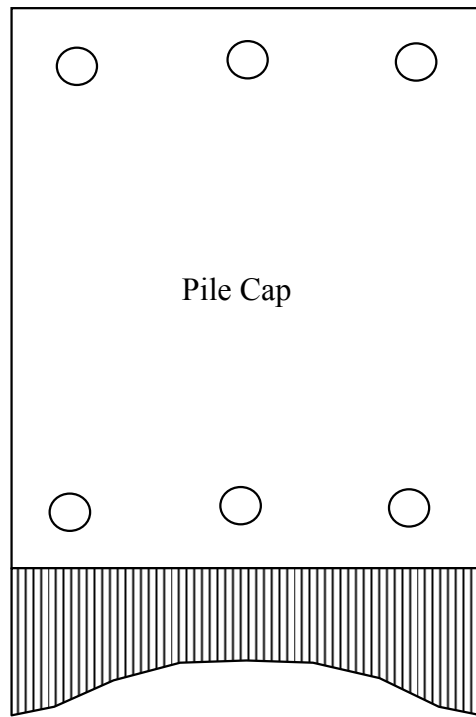


Figure 4-5 Schematic plan view drawing of pile cap showing stress concentrations at edges of the cap due to shear zones extending beyond the end of the cap and increasing the effective cap width

4.4 Results from Strain Gauges on MSE Steel Grid Reinforcements

The axial force in each steel reinforcing bar was computed by multiplying the measured strain at each strain gauge by the cross-section area of the bar and the elastic modulus of the steel. The total axial force for the grid was then computed by multiplying the force in the bar by the ratio of the total grid width to spacing between the bars (tributary width for one bar). The total force in the grid computed by this procedure is shown for the top and bottom reinforcements at three pile cap displacement increments during the pile cap test in Figure 4-6. In addition, the theoretical pull-out resistance as a function of distance along the length of the steel grid is shown on the plots in Figure 4-6 for comparison. When the pile cap had displaced only 0.6 inches into the backfill, the pullout force in both the steel grids was at or somewhat higher than the theoretical pull-out force within essentially all of the development length. This corresponds to the point when the wall panels started moving outward and the point where there was a plateau in the passive force-displacement curve for the pile cap as shown in Figure 4-2.

Unfortunately, it appears that the force in the steel grid near the wall face may be influenced by bending in the reinforcing which would artificially increase the measured force. Therefore, these forces are likely higher than they really are and account for the measured forces being significantly higher than the theoretical pullout force at distances close to the wall face. Bending stresses can be eliminated by having strain gauges on both top and bottom faces of the grid, but this doubles the cost of the strain gauges and/or reduces the number of points where force measurements can be made.

The forces in the reinforcing grids increase only slightly in most cases as the pile cap displacement increases. This is likely a result of the grids pulling out and allowing the wall to move outward so that the force in the steel grids remains essentially the same.

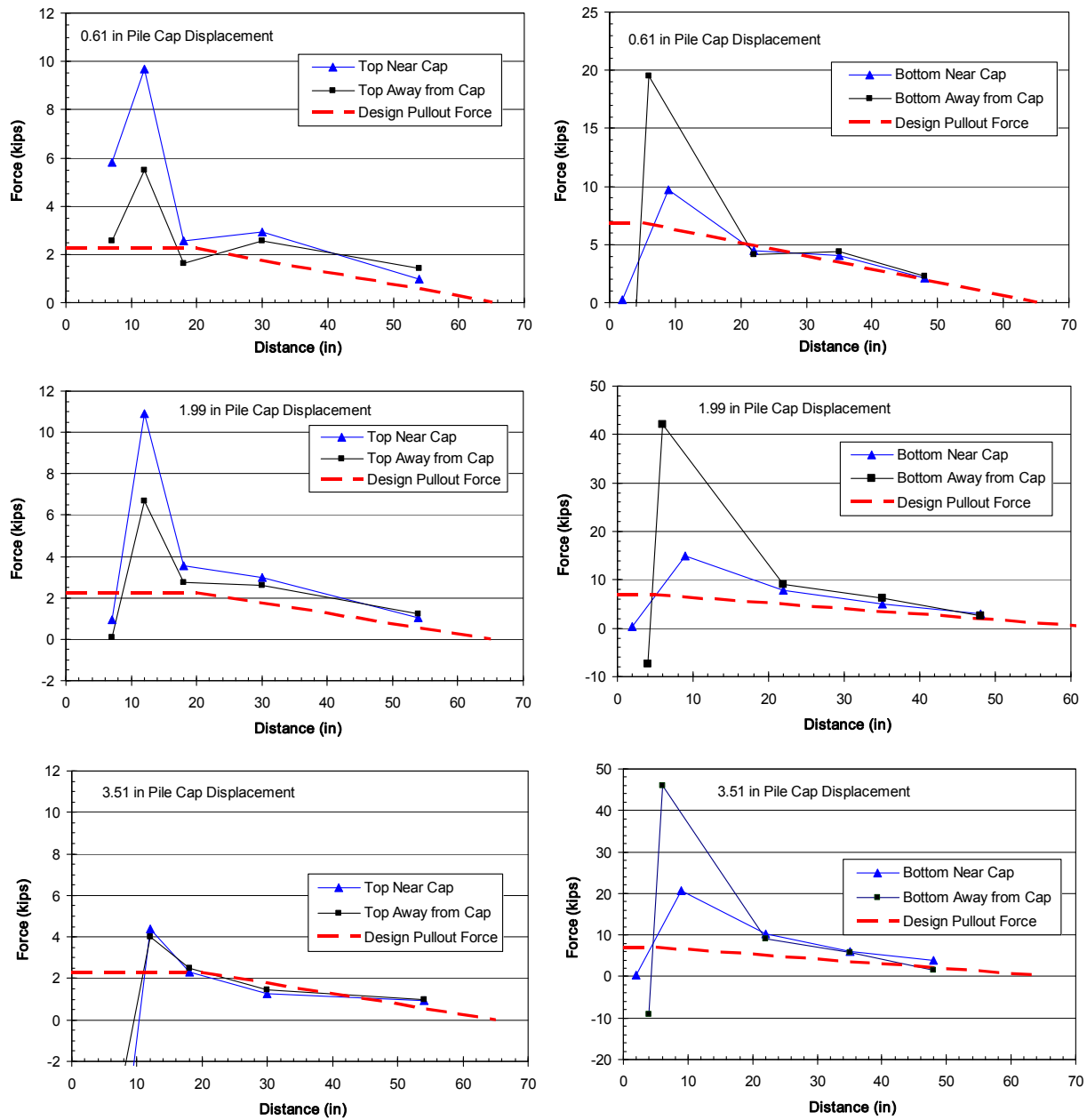


Figure 4-6 Summary of steel reinforcing grid force versus distance from the wall panel connection in comparison to the theoretical design pull-out force for top and bottom grids at pile cap displacements of 0.61, 1.99, and 3.51 inches.

A schematic diagram illustrating the mechanisms involved in increasing the force in the steel reinforcing grids is shown in Figure 4-7. As the pile cap is loaded into the backfill, passive pressure develops at the pile cap-backfill interface. The passive pressure and longitudinal displacement lead to a corresponding increase in pressure in the transverse direction. This pressure is resisted by increased force in the steel reinforcing grids which are holding the MSE wall in place. Once the pull-out force on the steel reinforcing grid is exceeded (i.e. the factor of safety against pullout is overcome), the wall simply moves laterally. As the pile cap continues to push into the backfill, the MSE wall continues to move outward, because no additional pull-out resistance is available. The author is not aware of any method currently available in the literature which would allow a designer to predict the magnitude of increased force which might develop on a MSE wall reinforcement as a result of loading of an abutment wall transverse to the reinforcement. Obviously, the overall pull-out factor of safety of 1.45 (1.08 and 1.66 for the individual factors of safety for the top and bottom grid panels, respectively) in this case was insufficient to prevent grid pull-out and displacement of the MSE wall. In retrospect increasing the factor of safety by using a heavier reinforcing grid or increasing the length of the panels, which would have meant increasing the width of the test pile cap, would likely have improved the test results by increasing the passive resistance due to the added confinement of the MSE wall. In general, increasing the factor of safety against pull-out would tend to reduce displacement of the MSE wall. However, increasing the stiffness of the wall in this manner might also attract additional pressure to the wall during the loading of the pile cap. To provide designers with some means of predicting the increased pressure on the MSE wall and restricting wall movement to acceptable levels, additional field testing would be desirable with walls having progressively higher factors of safety against reinforcement pull-out.

4.5 Compressive Movement of the Backfill and Transverse Movement of the MSE Wall

As noted previously, string potentiometers were attached to the face of the pile cap and then to steel stakes placed within the sand backfill for each test as seen in Figure 4-8. The stakes were placed at distances of 2, 6, 12, and 18 ft from the face of the pile cap. Figure 4-9 shows the

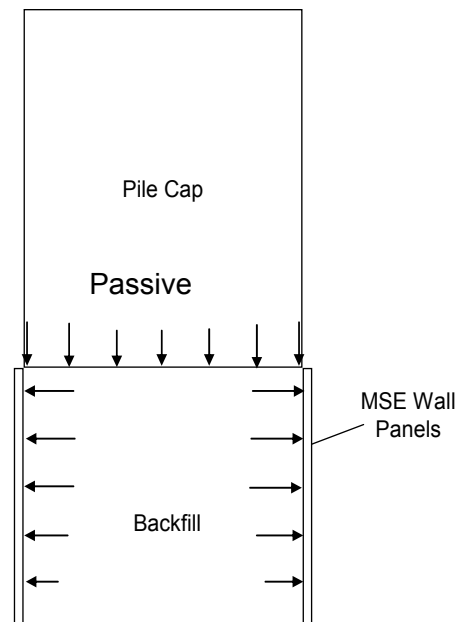


Figure 4-7 Schematic drawing showing how increased lateral pressure would be produced on the MSE wall as a result of longitudinal displacement and passive pressure development on the pile cap



Figure 4-8 Photograph of string potentiometers attached to steel stakes in backfill

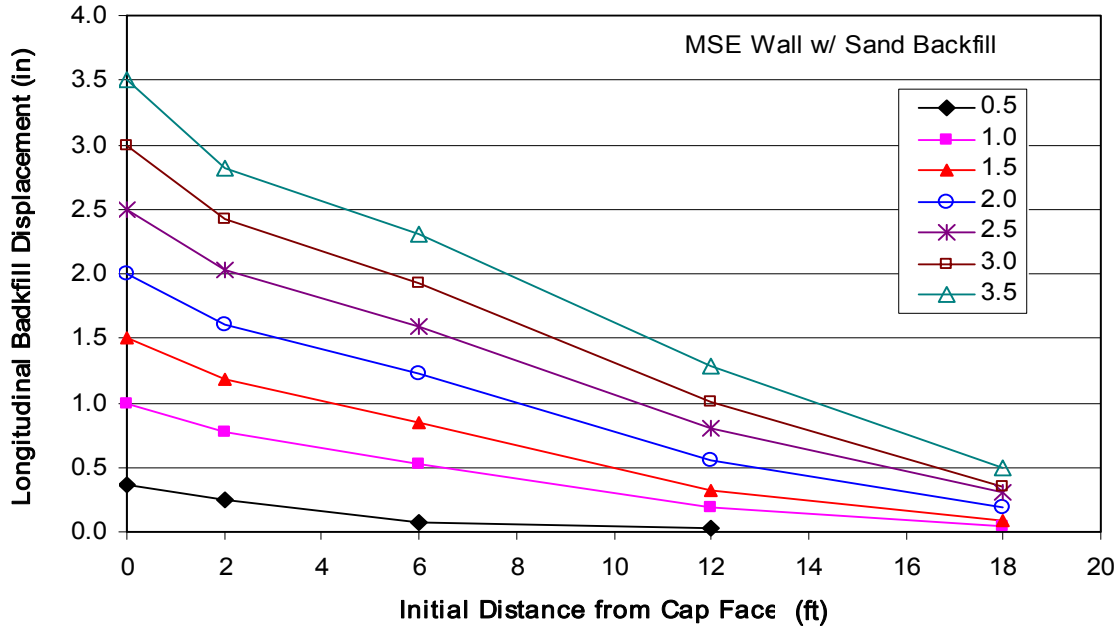


Figure 4-9 Longitudinal displacement of soil backfill as a function of initial distance from the pile cap face as the pile cap displaced longitudinally for MSE wall test

longitudinal displacement of the backfill, or lateral movement of the stake as it moved with the backfill, with distance from the cap during the progression of testing. This displacement occurred due to the deflection of the pile cap and compression of the backfill. As pile cap displacement increased, the backfill displacement increased and the slope of the displacement verses distance curve became steeper. Extrapolation suggests that the backfill displacement was close to zero at approximately 21 to 22 feet from the face of the pile cap. This distance is in reasonable agreement with failure surface lengths predicted by the log-spiral method.

A comparison of the longitudinal backfill displacement for the unconfined and MSE confined backfill soil is provided in Figure 4-10 for several pile cap displacement levels. The dashed lines represent soil displacement for the test with the MSE confined backfill while the

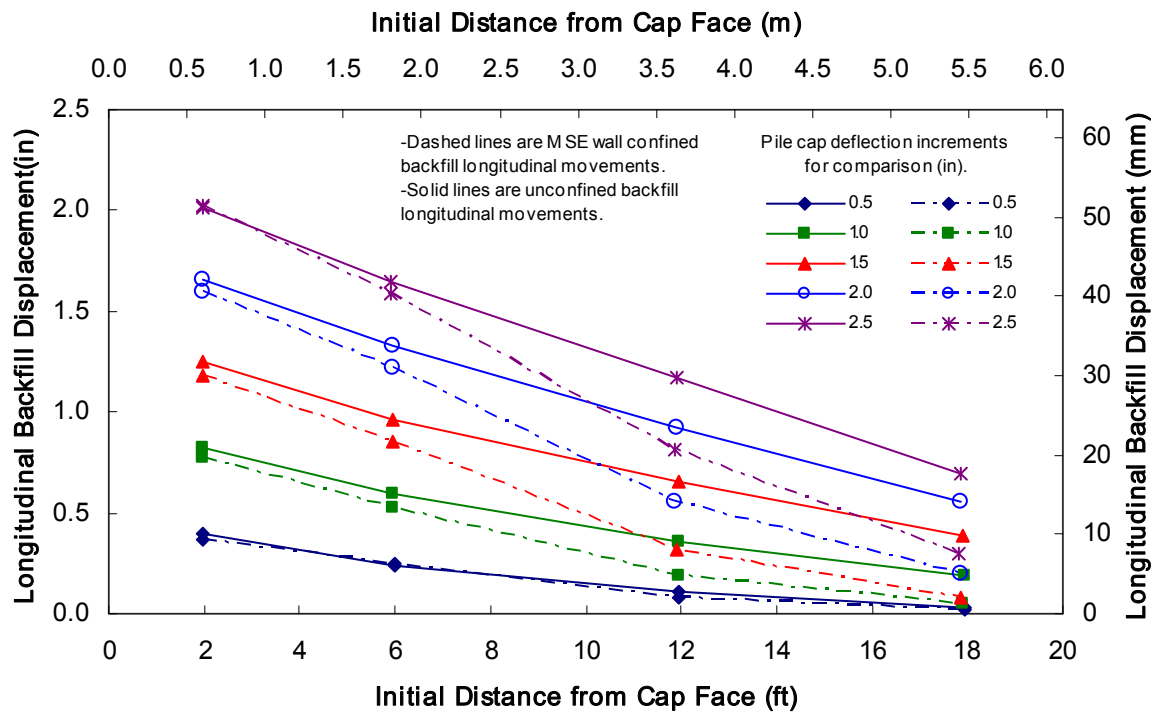


Figure 4-10 Longitudinal displacement of soil backfill for the MSE confined backfill (dashed lines) and unconfined backfill (solid lines) as a function of initial distance from the pile cap face as the pile cap deflected longitudinally.

solid lines represent soil displacement during the unconfined soil backfill test. For easier comparison, interpolated pile cap deflections at 0.5, 1.0, 1.5, 2.0, and 2.5 inches for each test were used instead of the incremental deflections mentioned earlier for each test. The plots in Figure 4-10 indicate that there was significantly less soil displacement in the sand backfill for the MSE wall confined test than for the test where the fill extended beyond the pile cap edges, particularly at distances of 12 and 18 ft behind the pile cap. This is most likely due to the transverse outward movement of the MSE walls themselves.

Figure 4-11 shows the displacement of the MSE walls transverse to the direction of loading as a function of distance from the pile cap face. Again, curves are plotted for each half

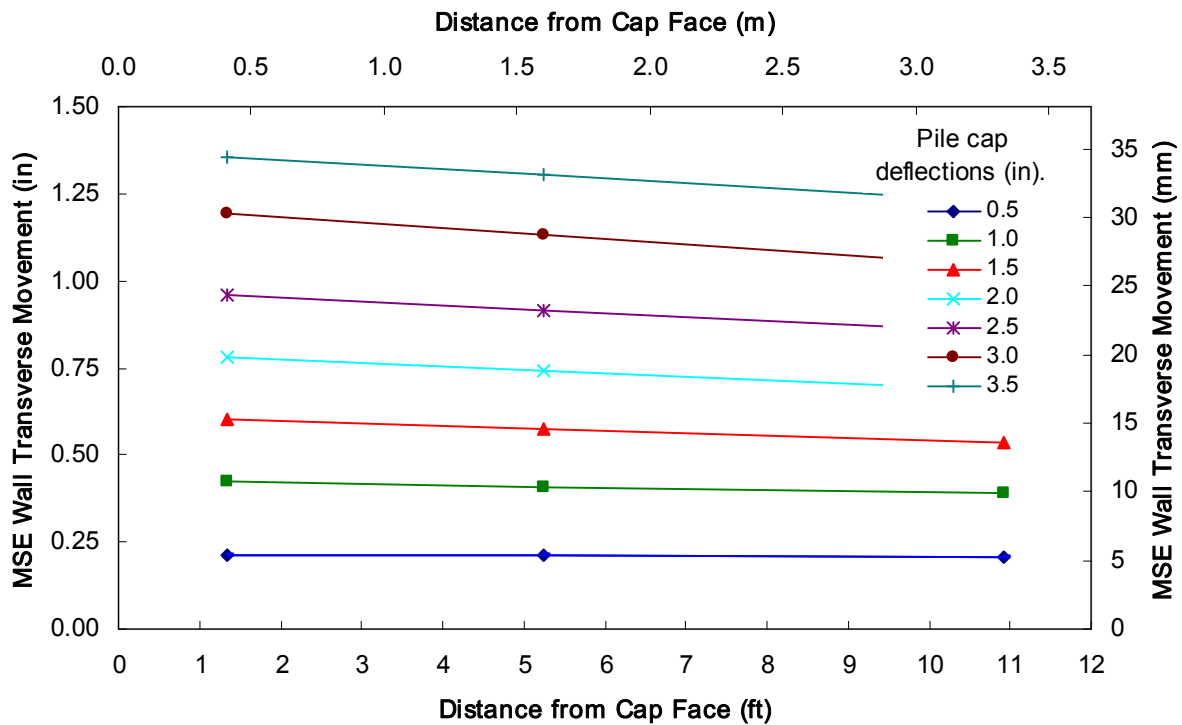


Figure 4-11 Displacement of the MSE wall panels transverse to the direction of loading as a function of distance from the pile cap face

inch longitudinal displacement of the pile cap to facilitate comparison with data in Figure 4-10. String potentiometers were attached to the pile cap and to steel stakes located at the center of the width in the sand backfill. Figure 4-11 shows that the entire instrumented MSE wall panel translated outward with the largest movement near the pile cap face. This behavior indicates that at large strains or displacements of the pile cap, the reinforcement strips began to pull through the sand backfill as the walls translated outward. The transverse wall displacement was typically about 40% of the longitudinal cap displacement. The maximum outward transverse movement of the MSE walls was 1.4 inches and occurred at a pile cap deflection of 3.50 inches. Wall movement was primarily translational, with relatively little rotation. Figure 4-12 and Figure 4-13 provide plots of the compressive strain in the backfill soil as a function of displacement from the

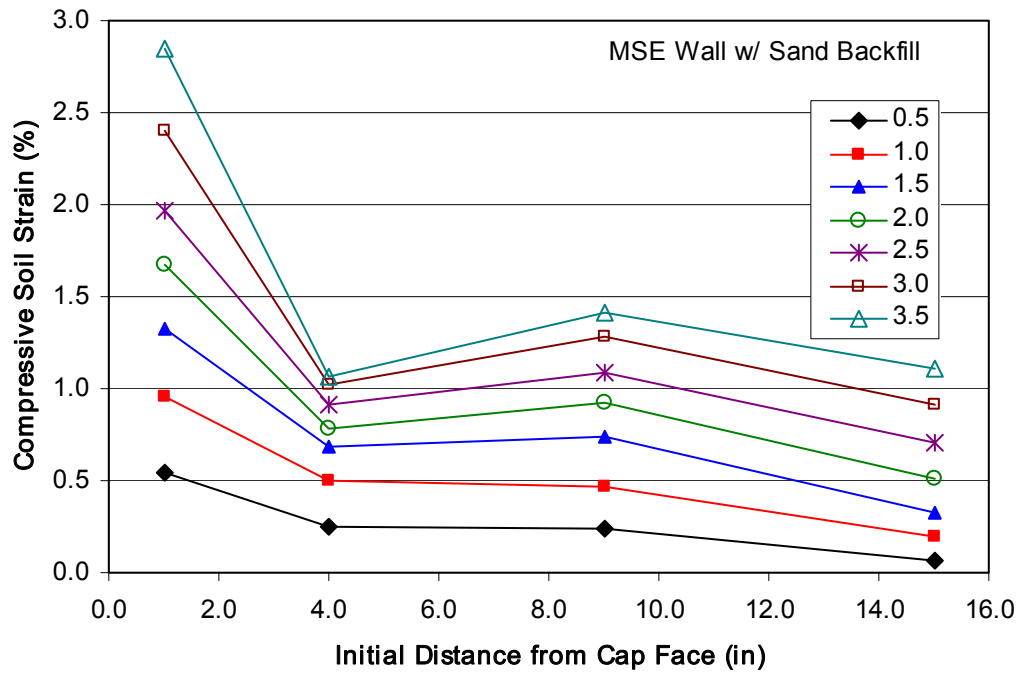


Figure 4-12 Compressive soil strain in the backfill confined by an MSE wing wall at various pile cap displacement levels

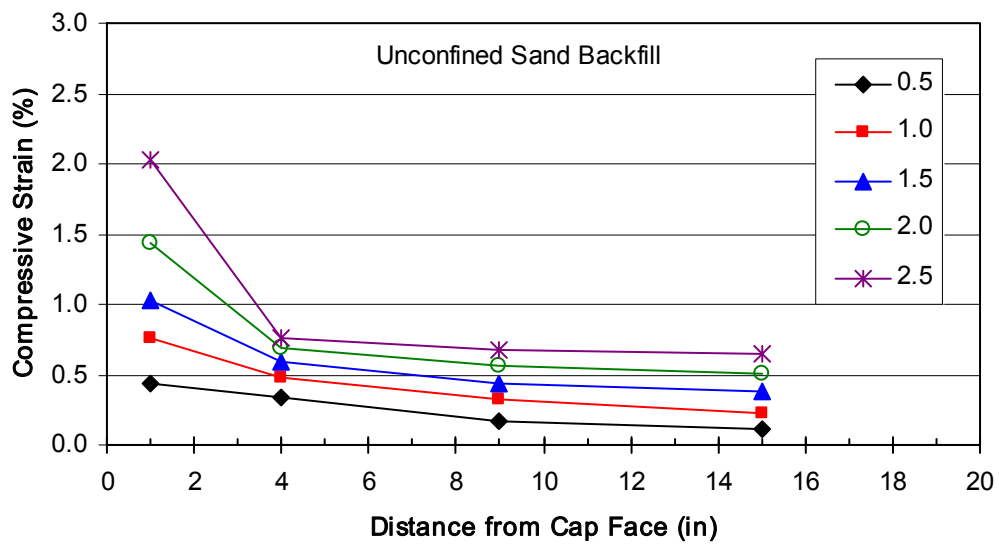


Figure 4-13 Compressive soil strain in the unconfined backfill at various pile cap displacement levels

pile cap face for the MSE wall confined backfill and for the unconfined backfill soils, respectively. Data is provided at each 0.5 inch longitudinal pile cap displacement. The strain was computed by subtracting the soil displacement between two measurement points (e.g. 0-2, 2-6, 6-12, 12-18 ft) and dividing by the initial distance between the two points. The average strain in each interval is plotted at the mid-point of the interval. As pile cap displacement increases, the compressive strain increases in all distance increments. However, the plots indicate that the greatest strain occurs in the 2 ft interval adjacent to the pile cap and then drops by a factor of two or more for subsequent distances. For the MSE wall test, maximum compressive strains reach about 3% adjacent to the cap at the ultimate state (at 3.5 inch cap displacement), but are typically between 1 and 1.5% at greater distances. For the test with unconfined backfill, maximum compressive strains only reach 2% adjacent to the pile cap at the ultimate state (at 2.5 inch cap displacement), while further out are about 0.75%.

A comparison plot of compressive strain as a function of distance from the pile cap face for unconfined backfill and backfill confined by MSE wing wall is provided in Figure 4-14 Comparison of compressive strain in the soil as a function of distance from the pile cap face for several pile cap displacement intervals (MSE confined backfill strain is shown with dashed lines while curves for unconfined backfill are shown with solid lines). The MSE confined backfill strain is shown with dashed lines while curves for unconfined backfill are shown with solid lines. Although the same trends are observed for both backfills, there is somewhat more strain at greater distances from the cap for the MSE confined backfill. This may be a result of the confinement of the MSE wall which would focus load further away from the pile cap.

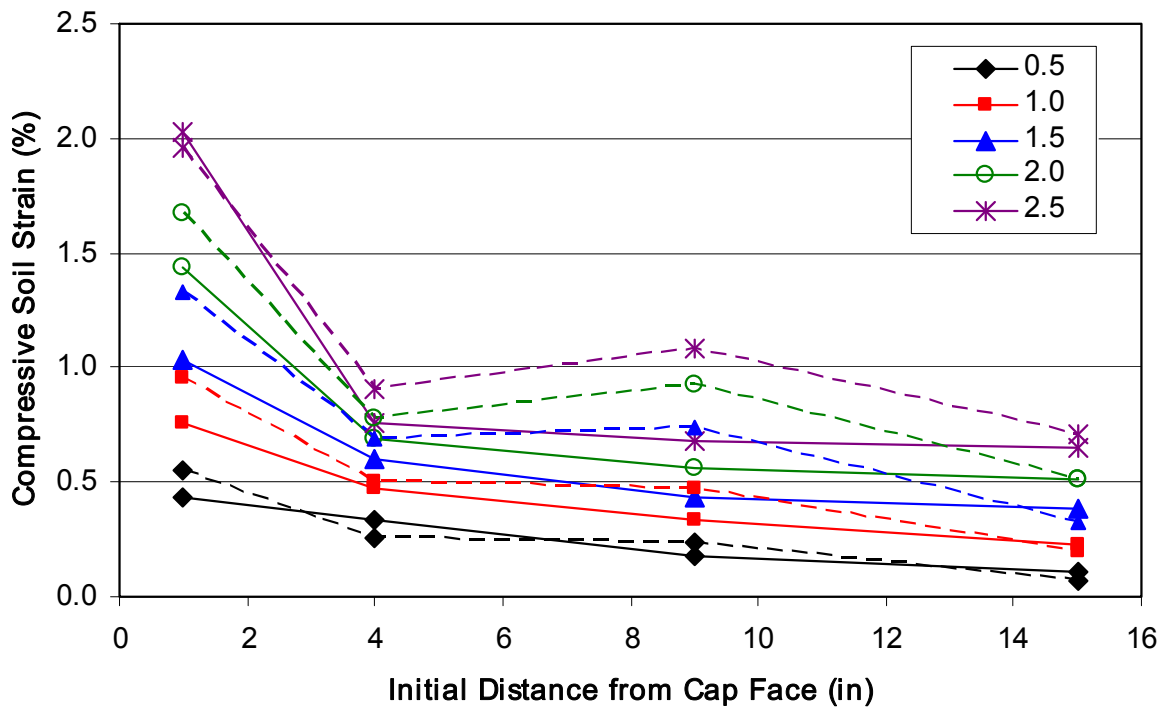


Figure 4-14 Comparison of compressive strain in the soil as a function of distance from the pile cap face for several pile cap displacement intervals (MSE confined backfill strain is shown with dashed lines while curves for unconfined backfill are shown with solid lines)

THIS PAGE INTENTIONALLY LEFT BLANK

5.0 COMPARISON WITH COMPUTED FORCE-DISPLACEMENT RESPONSE

The ultimate passive force was computed for both tests using the Rankine, Coloumb, log spiral and Caltrans methods for comparison with the measured ultimate force. Calculations were initially performed using a triaxial friction angle (ϕ_T) of 40.5° for both backfill geometries. Subsequently, calculations were also performed using a plane strain friction angle (ϕ_{ps}) of 43° for the backfill confined by MSE wing walls. For the confined backfill the cap width was 11 ft, while the effective width of the unconfined backfill was computed as 20.1 ft ($\phi_T=40.5^\circ$) using the Brinch-Hansen (1966) equation which accounts for 3D shear effects at the ends of the cap. This is about 10% higher than the effective width observed in the field testing. The wall friction was taken to be 0.72 times the friction angle which is slightly lower than that used by Rollins and Cole (2006). The moist unit weight was 116.4 lbs/ft³. Two log-spiral approaches were employed in this study. The first employs a moment equilibrium approach as recommended by Duncan and Mokwa (2001). The second uses a force equilibrium approach with a method of slides procedure as described by Shamsabadi, Rollins, and Kapaskur (2007). The Caltrans method was developed based on field tests of large-scale abutments 5.5 ft high with concrete wingwalls confining the soil backfill (Romstad et al 1996). For this wall height the Caltrans method computes the passive force as 5.5 kips/ft² times the area of the cap (Caltrans 2001).

A summary of the computed passive force using the various methods is provided in Table 5-1 Comparison of measured and computed peak horizontal passive force along with the measured passive force. After accounting for 3D shearing effects, the

Table 5-1 Comparison of measured and computed peak horizontal passive force

Peak Horizontal Force (kips)						
		Computed				
Backfill Type	Measured	Rankine	Coulomb	Log Spiral (Moment Eq.)	Log Spiral (Force Eq.)	Caltrans
Fill without MSE wing walls ($\phi_t=40.5^\circ$, $c=0$)	445	159	747	428	376 ($c=0$) 457 ($c=80$ psf)	298
Fill with MSE wing walls ($\phi_t=40.5^\circ$, $c=0$)	305	87	408	224	252 ($c=80$ psf)	298
Fill with MSE wing walls ($\phi_{ps}=43^\circ$, $c=0$)	305	99	652	301	303 ($c=40$ psf)	298

Rankine method still underestimated the ultimate passive force by a factor of 2.8 to 3.5, while the Coloumb method overestimated the ultimate passive resistance by 23% to 114%.

For the same friction angle, the log spiral method based on moment equilibrium typically yielded a passive force about 20% higher than predicted by the method based on force equilibrium. The inclusion of a small cohesion (40 to 80 psf) for the force equilibrium approach generally produced comparable results. Because the sand is partially saturated, evidence of apparent cohesion was observed during both field and lab testing. The log spiral methods, with allowance for shearing beyond the edge of the cap, provided excellent estimates of the ultimate passive force for the backfill without MSE wing walls. However, they underestimated the ultimate passive resistance for the backfill with MSE walls by 20 to 25% because they do not account for any confinement effects provided by the MSE wall. This discrepancy might be expected based on the geometry and behavior of the backfills discussed previously.

The unconfined backfill exhibited a crack pattern typical of a 3D or triaxial failure mode for which the triaxial friction angle was appropriate. In contrast, the backfill confined by the MSE wing walls was constrained to fail within a 2D geometry typical of a plane strain failure mode. For this situation a plane strain friction angle would be most appropriate and a lower triaxial friction angle would be expected to underestimate the measured resistance as was the case. The higher passive force could be adequately accounted for by using a higher plane strain friction angle (43°) rather than the triaxial friction angle (40.5°) which accounts for the failure geometry constrained by the MSE wall.

The Caltrans method provided an excellent estimate of the ultimate passive resistance for the MSE confined backfill, but underestimated the ultimate passive resistance for the unconfined backfill because it does not account for 3D shearing effects at the edges of the cap.

Passive force-displacement curves were computed using the hyperbolic method (Duncan and Mokwa 2001), the LSH method (Shamsabadi, Rollins and Kapaskur, 2007) and the Caltrans approach (Caltrans 2001). These curves are compared with the measured curves for the backfills with and without MSE walls in Figure 5-1 Comparison of measured and computed passive force versus deflection relationships for backfill without MSE walls (Calculations used triaxial friction angle) and Figure 5-2, respectively. The Caltrans method uses a linear stiffness of 20 kips/in per ft of pile cap width up to the ultimate passive force. The Duncan and Mokwa (2001) hyperbolic method uses an initial stiffness based on the elastic modulus which was taken as 800 kip/ft^2 based on previous studies (Cole and Rollins 2006). Displacement at failure was taken as 3% of wall height for the unconfined backfill and 4.2% of wall height for the confined backfill. Poisson's ratio was assumed to be 0.3. For the LSH hyperbolic method, the ϵ_{50} was assumed to be 0.002 based on recommendations from Shamsabadi et al (2007).

The hyperbolic and LSH methods provided a reasonable estimate of the initial stiffness of the backfill in both cases as well as the ultimate force; however, neither method was successful

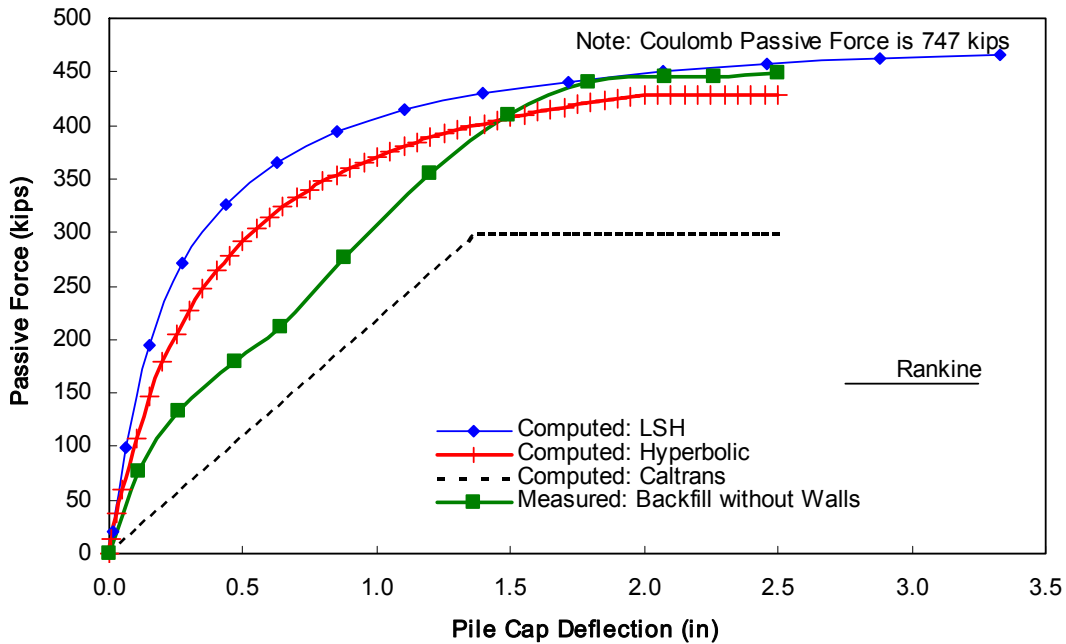


Figure 5-1 Comparison of measured and computed passive force versus deflection relationships for backfill without MSE walls (Calculations used triaxial friction angle)

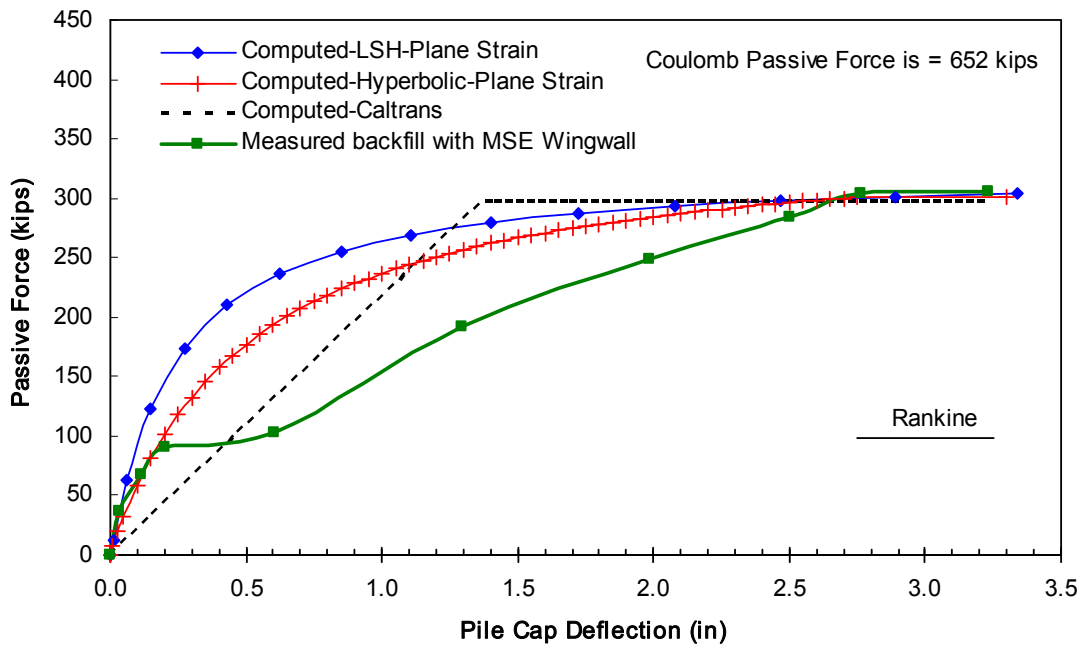


Figure 5-2 Comparison of measured and computed passive force versus deflection relationships for backfill confined by MSE wing walls (Calculations used plane strain friction angle)

in matching the overall shape of the measured response. This is likely due to the flattening of the curve due to the cyclic loading at each load increment. The agreement was particularly poor for the backfill confined with MSE wing walls. In this case, the outward movement of the MSE walls resulting from grid pull-out appears to have significantly reduced the stiffness, although the ultimate load was eventually achieved at larger displacements. For the two cases investigated, the LSH provided a somewhat higher load at a given displacement than the other hyperbolic method. The Caltrans method underestimated the initial stiffness by a factor of two for the unconfined backfill, but was stiffer than the curve for the backfill with MSE wing walls. This would probably not have been the case if the MSE walls had not moved outward, because the initial measured stiffness was higher than the computed value (see Figure 5-2).

THIS PAGE INTENTIONALLY LEFT BLANK

6.0 RESPONSE TO CYCLIC AND DYNAMIC LOADINGS

The resistance of the pile cap with the MSE wall backfill in place during small amplitude cyclic and dynamic loading was analyzed by isolating the test setup north of the actuators shown in Figure 2-1. To the north of the actuators, the only forces to be considered are those affecting the pile cap and MSE walled backfill. These forces consist of the actuator force; the shaker force; the stiffness, damping, and inertial forces from the cap by itself; and the stiffness, damping, and inertial forces from the backfill materials. The net stiffness, damping, and inertial forces from the reaction foundation system are accounted for by the actuator loads.

The inertial force for the pile cap system was calculated using measured acceleration data from the cap and a constant, single lumped-mass representation of the test pile cap, shaker, a portion of the piles (the upper eight pile-diameters), one of the actuators, and the backfill. The inertial force was combined with the shaker and actuator forces such that the resulting force-displacement loops represent the combined internal stiffness and damping effects of the pile cap system. Stiffness of the resulting system force-displacement loops were subsequently analyzed as a function of both displacement level and load frequency. Dynamic stiffness, k , was calculated using the average peak-to-peak slope for the force-displacement loops experienced during the dwell time at each 0.5 Hz loading increment. Because the shaker provides an increasing excitation force to the pile cap with increasing frequency, in order to fairly compare the resulting dynamic displacement amplitudes, plots of displacement amplitude normalized by the shaker force (which is in turn proportional to the square of the frequency) have also been provided.

Damping during cyclic and dynamic loading, ξ , was evaluated directly from the force-displacement loops using the Equation 6-1, as follows:

$$\xi = \frac{1}{4\pi} \frac{A}{E_s} \quad (6-1)$$

where A is the area of the resistance force-displacement loop; and E_s is the stored strain energy which equals $0.5 k u_o^2$, in which case k is the slope of the loop, and u_o is its displacement amplitude.

The response of the pile cap with a full width of densely compacted sand and with MSE walled backfill to the cyclic actuator loadings is shown in Figure 6-1 Summary of pile cap response to cyclic actuator loadings with either the MSE walled backfill or with the backfill extending beyond the edges of the pile cap. The displacement amplitudes of the cyclic loadings were typically 0.06 inches with the MSE wall present and 0.04 inches without. It can be seen in the figure that the presence of the MSE wall decreases the stiffness of the pile cap by approximately 50% relative to the backfill extending beyond the edges of the pile cap. These changes in stiffness directly affect the calculated natural frequencies of the pile cap, which range from 5.3 to 8.3 Hz and from 6.7 to 10 Hz with and without the MSE wall present, respectively. In both cases, frequency increases with increasing pile cap displacement. Although the average areas of individual load-displacement loops remain relatively constant for the full range of static displacement levels, damping decreases due to the increasing stiffness, with a range of 0.25 to 0.15 during low frequency cyclic loadings.

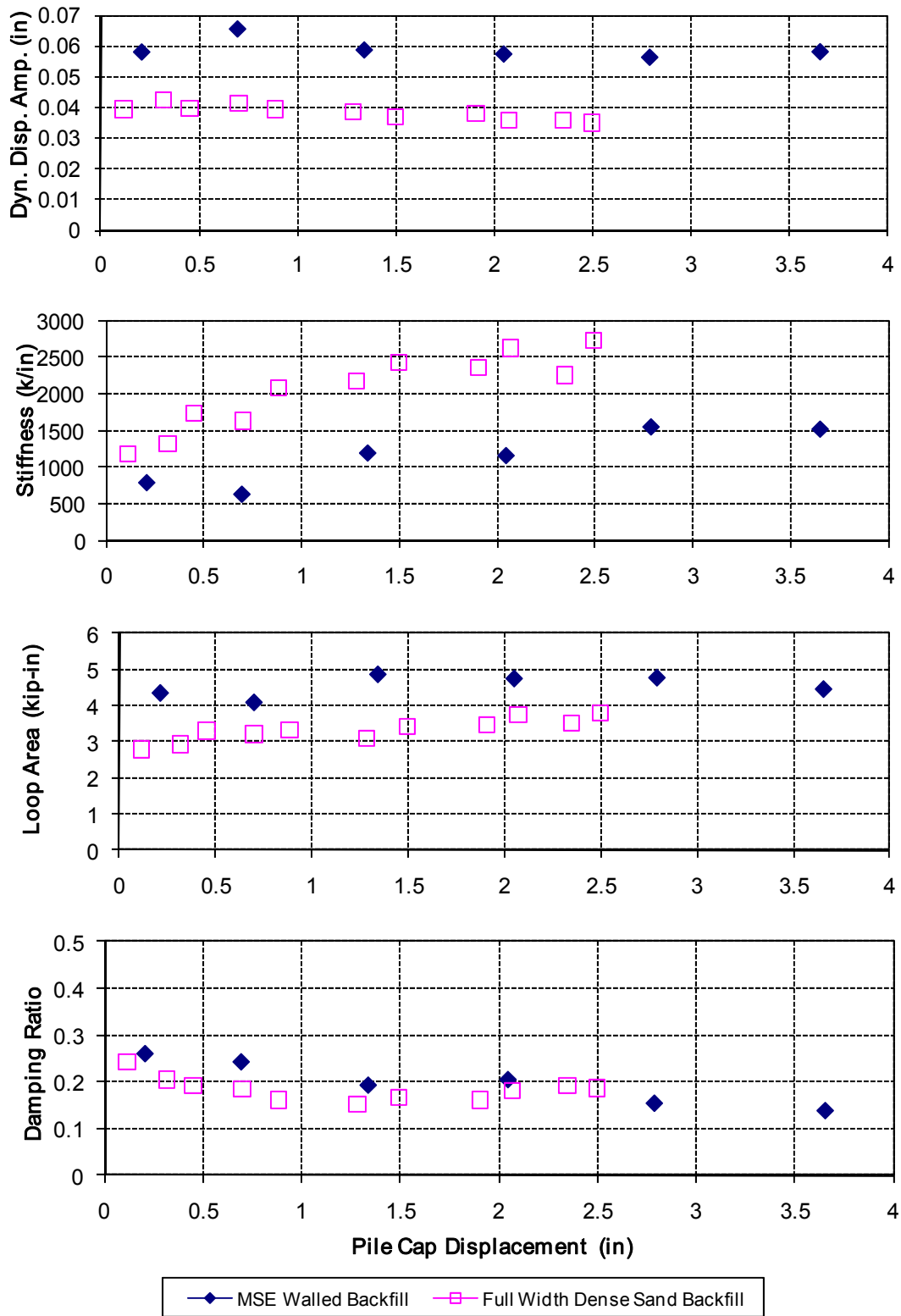


Figure 6-1 Summary of pile cap response to cyclic actuator loadings with either the MSE walled backfill or with the backfill extending beyond the edges of the pile cap

The response of the pile cap with backfill extending beyond its edges and with the MSE wall truncated backfill to the dynamic shaker loadings is shown in Figure 6-2. In this figure, data is shown for static displacements of approximately 2 inches in which the shaker was used before cycling the actuators, which corresponds to the eighth displacement level (i.e. dynamic test) conducted in the densely compacted clean sand backfill and the fourth displacement level (i.e. dynamic test) conducted with the MSE walled backfill. Unfortunately, due to the nature of variable force testing with a shaker, large forces, and hence large pile cap displacements, values cannot be produced at low frequencies. Consequently, values computed for frequencies of less than 3 to 4 Hz appear to be unreliable because of the difficulty in distinguishing real signals from instrument noise. Results from the cyclic actuator loadings at 0.75 Hz have been substituted for this data.

In order to properly interpret the response data shown in the figure, one must remember that the response is the composite behavior of the test pile cap and the backfills and that the phase of each relative to the other varies throughout the test. One of the primary features of the figure is the variation of stiffness with frequency. For both backfills, stiffness increases up to a frequency of about 5 or 6 Hz, after which it decreases dramatically to levels lower than its initial low frequency (i.e. static) value. This behavior is interpreted as the relative motions of the backfill and pile cap initially combining to increase stiffness, after which their relative phases change and the net stiffness decreases. This is not to say that the individual stiffness of the cap or backfill change (although some softening may be present), but rather the manner in which they combine in time produces the observed behavior. When the pile cap and MSE wall backfill are acting in concert, there is an 80% increase in dynamic stiffness, and there is a 60% net

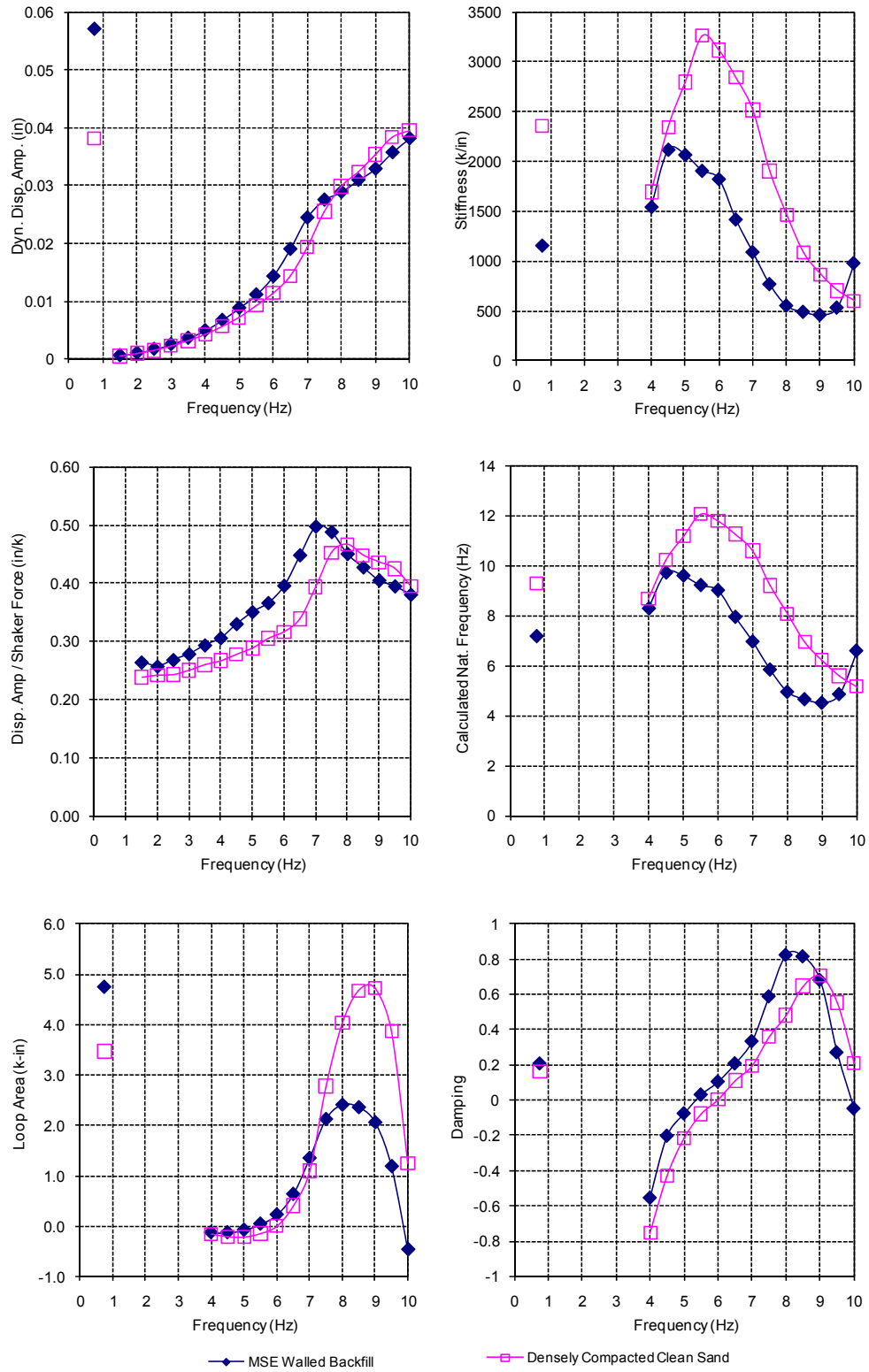


Figure 6-2 Summary of pile cap response to dynamic shaker loadings with either an MSE walled backfill or with backfill extending beyond the pile cap edge

decrease when not. For the densely compacted clean sand, the increase and decrease are 45 and 55%, respectively.

The net damping behavior is also strongly dependent on the relative interaction of the pile cap and backfill. Note that the figure shows negative damping values between approximately 4 and 6 Hz. The negative sign results from the very small negative area of the force-displacement loop, where a negative value means a reversal of loading direction. Because of the size of the loop, the accuracy of the computed damping is somewhat suspect; however, in general, the negative damping shown here can also be simply interpreted as a reversal in the direction of the net damping force (and the magnitude of the damping force is proportional to the absolute value of the damping shown in the figure). Damping is near zero where the net stiffness is the greatest, with the damping of the cap and backfill having combined to produce a very linear load-displacement response whose enclosed loop area is negligible. At higher frequencies, as stiffness decreases, the damping increases.

7.0 CONCLUSIONS

Based on the test results and analysis relative to the large-scale field tests on the backfills with and without MSE wing walls, the following conclusions have been developed:

1. During lateral loading of the unconfined backfill, shear zones extended about 3 to 3 1/2 ft beyond the edge of the cap increasing the effective cap width from 11 ft to approximately 18 to 19 ft.
2. Lateral loading of the pile cap produced increased soil pressure on the MSE wing walls which induced pull-out of the steel grids. Outward transverse displacement of the MSE wall was typically about 40% of the longitudinal displacement of the pile cap. The outward movement significantly reduced the stiffness of the pile cap load-displacement curve and required more longitudinal movement to develop the ultimate passive force.
3. The ultimate passive force for the MSE wall confined backfill was 24% lower than for the unconfined backfill primarily due to the reduced effective width of the cap. However, confinement did increase the ultimate passive force above what would be expected based on the width of the pile cap. The ultimate passive force per width was 28 kips/ft and 25 kips/ft for the MSE confined and unconfined walls, respectively.
4. The log spiral methods, with allowance for shearing beyond the edge of the cap, provided an excellent estimate of the ultimate passive resistance for the unconfined backfill. However, using a triaxial friction angle they underestimated the ultimate passive resistance for the MSE confined backfill by 20 to 25%. To obtain reasonable agreement with measured results it was necessary to use a higher plane strain friction angle with accounts for the confinement and 2D failure geometry imposed by the MSE wall.
5. The Caltrans method, which was developed based on tests involving concrete wing walls, provided an excellent estimate of the ultimate passive resistance for the MSE wall

confined backfill, but underestimated the ultimate passive resistance for the backfill extending beyond the width of the pile cap because it does not account for 3D shearing effects at the edge of the cap.

6. After accounting for 3D shearing effects, the Rankine method still underestimated the ultimate passive force by a factor of 2.8 to 3.5, while the Coloumb method overestimated the ultimate passive resistance by 33% to 114%.
7. The hyperbolic methods provided a reasonable estimate of the initial stiffness of the backfill, while the Caltrans method underestimated the initial stiffness by a factor of two. Neither method matched the measured curve throughout the entire loading cycle.
8. The natural frequency of the pile cap shifted from approximately 5.3 to 8.3 Hz as the cap with MSE walled backfill was statically displaced into the backfill; the frequency shifted from approximately 8.3 to 10 Hz when the densely compacted sand backfill is extended beyond the edge of the pile cap width.
9. Damping ratios were typically between 15 and 20% for the cyclic actuator tests.
10. When the pile cap and MSE wall backfill are reacting in concert under dynamic loading, there is an 80% increase in stiffness, and there is a 60% net decrease when they are not. For the densely compacted clean sand, the increase and decrease in dynamic stiffness is 45 and 55%, respectively.

8.0 RECOMMENDATIONS

The ultimate passive force for abutments with MSE wing walls should be computed using the log spiral method which is in agreement with recent AASHTO code recommendations. In making the calculation of the passive earth pressure coefficient, the wall friction can be assumed to be 70% to 75% of the soil friction angle and the plane strain friction angle should be used rather than the triaxial friction angle. The plane strain friction angle can be approximated by increasing the triaxial friction angle by about 10%, which will typically increase the friction angle by 3 to 4 degrees. This will typically lead to a much higher ultimate passive force. Based on these and other tests the ultimate passive force can be estimated to develop after a displacement of about 4 to 5% of the wall height.

Typically, the passive force-displacement is not simply linear but has a hyperbolic curve shape. This curve shape can typically be computed using the computer models PYCAP and ABUTMENT with reasonable accuracy. However, results from this study suggest that the curve shape is significantly flattened by MSE reinforcement pull-out. Additional testing tests should be undertaken with MSE wing walls to develop a method to predict the pressure applied to the MSE wall as the passive force is applied to the abutment. At present there is no design procedure which can be used to adequately design the MSE walls for pull-out during this loading condition.

THIS PAGE INTENTIONALLY LEFT BLANK

9.0 REFERENCES

- Brinch Hansen, J. (1966). "Resistance of a rectangular anchor slab." *Bulletin No. 21*. Danish Geotechnical Institute, Copenhagen, pp. 12-13.
- Caltrans (2001). "Seismic design criteria version 1.2." *California Department of Transportation, Sacramento, California*.
- Christensen, D.L. (2006). "Full-scale lateral load test of a 3x3 pile group in sand." *MS Thesis*, Civil & Environ. Engrg. Dept., Brigham Young Univ., Provo, UT, pp. 182.
- Cole, R.T and Rollins, K.M. (2006). "Passive Earth Pressure Mobilization During Cyclic Loading." *J. Geotechnical and Geoenvironmental Engrg.*, Vol. 132 (9): 1154-1164.
- Duncan, J.M. and Mokwa, R. L. (2001). "Passive earth pressures: theories and tests." *J. Geotechnical and Geoenv. Engrg.*, ASCE, Vol. 127 (3): 248-257.
- El-Gamal, M. and Siddharthan, R.V. (1998). "Stiffness of Abutments of Piles in Seismic Bridge Analyses." *Soils and Foundations*, JGS, Vol. 38 (1): 77-87.
- Faraji, S. Ting, J.M., Crovo, D.S., and Ernst, H. (2001). "Nonlinear analysis of integral bridges; finite-element model." *J. Geotechnical & Geoenviron. Engrg.*, ASCE, Vol. 127 (5): 454-461.

- FHWA (1999). "Mechanically Stabilized Earth Walls and Reinforced Soil Slopes Design and Construction Guidelines." *Federal Highway Administration* Publication No. FHWA A-SA-96-071.
- Mokwa, R. L. and, Duncan, J. M., (2001). "Experimental evaluation of lateral-load resistance of pile caps." *J. Geotechnical and Geoenv. Engrg.*, ASCE Vol. 127, (2): 185-192.
- Peterson, K.T. and Rollins, K.M. (1996). "Static and dynamic lateral load testing of a full-scale pile group in clay", Civil Engineering Dept. Research Report CEG.96-02, Brigham Young University, Provo, Utah.
- Rollins, K. M. and Cole, R. T., (2006). "Cyclic Lateral Load Behavior of a Pile Cap and Backfill" *J. Geotechnical and Geoenv. Engrg.*, ASCE Vol. 132 (9): 1143-1153.
- Rollins, K.M. and Sparks, A.E. (2002) "Lateral Load Capacity of a Full-Scale Fixed-Head Pile Group." *J. Geotechnical and Geoenv. Engrg.*, ASCE, Vol. 128 (9): 711-723.
- Romstad, K. Kutter, B., Maroney, B., Vanderbilt, E. Griggs, M. and Chai, Y.H. (1996). "Longitudinal Strength and Stiffness Behavior of Bridge Abutments" Dept. of Civil and Environ. Engrg., Univ. of California-Davis, Report No. UCD-STR-96-144 p.
- Shamsabadi, A., Rollins, K.M., Kapaskur, M. (2007). "Nonlinear Soil-Abutment-Bridge Structure Interaction for Seismic Performance-Based Design." *J Geotechnical and Geoenv.*, ASCE, Vol. 133 (6): 707-720.
- Snyder, J.L. (2004). "Full-scale lateral load test of a 3x5 pile group in soft clays and silts." *MS Thesis*, Civil & Environ. Engrg. Dept., Brigham Young Univ., Provo, UT, 220 p.

APPENDIX

A. Calculation showing factor of safety for MSE wall grid against pull-out failure

Depth (ft)	K_a	K	σ_v (psf)	σ_H (psf)	x-bar	x-bar spacing (in.)
1.79	0.22	0.52	202.38	104.81	W8	12
4.29	0.22	0.48	484.76	233.64	W8	12

F*	α	L_t (ft)	L_e (ft)	C	Pr (lb/ft)	Bar Mat Width (in.)
0.50	1.00	5.50	3.85	2.00	774.67	32
0.46	1.00	5.50	4.78	2.00	2148.33	32

Pr (lb)	At (ft ²)	T (lb)	F.S.	
2065.80	18.25	1912.71	1.08	Top Reinforcement
5728.89	14.75	3446.25	1.66	Bottom Reinforcement

Total Force on Panel: 10718 (lb)
 Total Resistance From Panel: 15589 (lb)
 Panel Factor of Safety: 1.45

- K_a = Active pressure coefficient
- K= Variation of stress with depth coefficient
- σ_v = Vertical stress
- σ_H = Horizontal stress
- x-bar= panel type
- F*= Pullout resistance factor
- α = Scale correction factor
- L_t = Total grid length
- L_e = Length of embedment in resisting zone
- C= Coefficient (2 for strip, grid and sheet type reinforcement)
- Pr= Pullout resistance
- At= Tributary panel area
- T= Horizontal force on tributary area

B. Calculation showing grid steel yield check

Factor of safety, FS= 0.48 See Publication No. FHWA A-SA-96-071 (1999) p. 75
 Design cross-section area of grid, A_c = 0.55 in²
 Yield stress of steel, F_y = 36000 psi
 Allowable tensile force per grid, T_a = 9543 (FS* A_c * F_y /b)
 >
 Max T above= 3447 OK